

# WINGS-SPE III: Equivalent width measurements, spectral properties and evolution of local cluster galaxies. \* \*\*

J. Fritz<sup>1</sup>, B. M. Poggianti<sup>2</sup>, A. Cava<sup>3</sup>, A. Moretti<sup>4,2</sup>, J. Varela<sup>5</sup>, D. Bettoni<sup>2</sup>, W. J. Couch<sup>6,7</sup>, M. D’Onofrio<sup>4</sup>,  
A. Dressler<sup>8</sup>, G. Fasano<sup>2</sup>, P. Kjærgaard<sup>9</sup>, P. Marziani<sup>2</sup>, M. Moles<sup>5</sup>, and A. Omizzolo<sup>2,10</sup>.

- <sup>1</sup> Sterrenkundig Observatorium Vakgroep Fysica en Sterrenkunde Universiteit Gent, Krijgslaan 281, S9 9000 Gent  
e-mail: [jacopo.fritz@UGent.be](mailto:jacopo.fritz@UGent.be)  
<sup>2</sup> INAF-Osservatorio Astronomico di Padova, vicolo Osservatorio 5, 35122 Padova, Italy  
<sup>3</sup> Observatoire de Genève, Université de Genève, 51 Ch. des Maillettes, 1290 Versoix, Switzerland  
<sup>4</sup> Dipartimento di Astronomia, vicolo Osservatorio 2, 35122 Padova, Italy  
<sup>5</sup> Centro de Estudios de Física del Cosmos de Aragón (CEFCA), Plaza San Juan 1, planta 2, E-44001 Teruel, Spain  
<sup>6</sup> Centre for Astrophysics and Supercomputing, Swinburne University of Technology, Melbourne Australia  
<sup>7</sup> Australian Astronomical Observatory, Sydney Australia  
<sup>8</sup> Observatories of the Carnegie Institution of Washington, Pasadena, CA 91101, USA  
<sup>9</sup> Niels Bohr Institute, Juliane Maries Vej 30, 2100 Copenhagen, Denmark  
<sup>10</sup> Specola Vaticana, 00120 Stato Città del Vaticano

Received ...; accepted ...

## ABSTRACT

**Context.** Cluster galaxies are the ideal sites to look at when studying the influence of the environment on the various aspects of galaxies’ evolution, such as the changes in their stellar content and morphological transformations. In the framework of WINGS, the WIde-field Nearby Galaxy-cluster Survey, we have obtained optical spectra for  $\sim 6000$  galaxies selected in fields centered on 48 local ( $0.04 < z < 0.07$ ) X-ray selected clusters to tackle these issues.

**Aims.** By classifying the spectra based on given spectral lines, we investigate the frequency of the various spectral types as a function both of the clusters’ properties and of the galaxies’ characteristics. In this way, using the same classification criteria adopted for studies at higher redshift, we can consistently compare the properties of the local cluster population to those of their more distant counterparts.

**Methods.** We describe a method we have developed to automatically measure the equivalent width of spectral lines in a robust way even in spectra with a non optimal signal to noise. Like this, we can derive a spectral classification reflecting the stellar content, based on the presence and strength of the [OII] and H $\delta$  lines.

**Results.** After a quality check, we are able to measure 4381 of the  $\sim 6000$  originally observed spectra, in the fields of 48 clusters, 2744 of which are spectroscopically confirmed cluster members. The spectral classification is then analyzed as a function of galaxies’ luminosity, stellar mass, morphology, local density and host cluster’s global properties, and compared to higher redshift samples (MORPHS and EDisCS). The vast majority of galaxies in the local clusters population are passive objects, being also the most luminous and massive. At a magnitude limit of  $M_V < -18$ , galaxies in a post-starburst phase represent only  $\sim 11\%$  of the cluster population and this fraction is reduced to  $\sim 5\%$  at  $M_V < -19.5$ , which compares to the 18% at the same magnitude limit for high- $z$  clusters. “Normal” star forming galaxies ( $e(c)$ ) are proportionally more common in local clusters.

**Conclusions.** The relative occurrence of post-starbursts suggests a very similar quenching efficiency in clusters at redshifts in the 0 to  $\sim 1$  range. Furthermore, more important than the global environment, the local density seems to be the main driver of galaxy evolution in local clusters, at least with respect to their stellar populations content.

**Key words.** galaxies: clusters: general - galaxies: stellar content - galaxies: evolution - methods: data analysis

## 1. Introduction

It is now widely accepted that the evolution of galaxies’ properties such as morphology, gas and dust content and stellar population properties, has a very strong dependence on the environment where galaxies are found. Galaxies we observe in local clusters and in the field not only present different characteristics, but also the way that led them to be as we observe them now, that is their evolution, is different. By evolution, in this context, we mean the transformations that galaxies undergo both from the morphological aspect

Send offprint requests to: Jacopo Fritz,  
e-mail: [jacopo.fritz@UGent.be](mailto:jacopo.fritz@UGent.be)

\* Based on observations taken at the Anglo Australian Telescope (3.9 m- AAT), and at the William Herschel Telescope (4.2 m- WHT)

\*\* Table A.1 is available in electronic form both at the CDS via anonymous ftp to [cdsarc.u-strasbg.fr](ftp://cdsarc.u-strasbg.fr) (130.79.128.5) or via <http://cdsweb.u-strasbg.fr/cgi-bin/qcat?J/A+A/????/????>, and by querying the WINGS database at <http://web.oapd.inaf.it/wings/new/index.html>

and with respect to their stellar population content, as a function of the cosmic time.

A striking example of this environmental dependency is the paucity of blue, late-type galaxies at the centre of local clusters, at odd with what it was found in higher redshift rich clusters where a large population of blue, star-forming galaxies was already discovered more than 3 decades ago (Butcher & Oemler, 1978a,b, 1984). This is one of the most clear examples of the consequences of the evolutionary effects observable in galaxies in dense environments, and evidences for it have been gathered during the following years (see, among the others, Couch et al., 1994; Lavery et al., 1992; Margoniner & de Carvalho, 2000; De Propriis et al., 2003, 2004; Haines et al., 2009).

Since then, galaxy clusters have proved to be a very important place to study galactic evolution, and were used to probe an extremely wide range of physical conditions, from the dense cores, to the outermost, low-density regions. This was achieved, during the past years, both from a morphological perspective (see, e.g., Hausman & Ostriker, 1978; Dressler, 1980; Buote & Tsai, 1995; Dressler et al., 1997; Fasano et al., 2000; van Dokkum & Franx, 2001; Goto et al., 2004; Sánchez-Blázquez et al., 2009; Poggianti et al., 2009a) and from the point of view of the stellar populations hosted by these galaxies (e.g. Couch & Sharples, 1987; Dressler & Gunn, 1983, 1992; Dressler et al., 1999; Postman et al., 2001; Dressler et al., 2013; Gladders et al., 2013).

Furthermore, evidences are already in place since many years for the fact that the cluster environment acts not only on a “global” scale, but also “locally”. Prugniel et al. (1999), e.g., demonstrated how the presence of young stellar populations is affected by the local environment, showing that galaxies hosting recent star formation tend to prefer the less dense environment of the field or of poor groups. On the other side, the emission-line galaxies fraction was found to decrease towards the centre of dense clusters (e.g. Biviano et al., 1997; Dale et al., 2001), proving the importance of the local conditions. Similarly, the projected distance from the cluster’s centre was found to be the main factor driving the differences between passive ellipticals and actively star forming spirals (see Thomas & Katgert, 2006, and references therein), proving the importance of the global environment.

The best approach when trying to understand how blue, actively star forming galaxies so common in high-redshift galaxy clusters, turn into red and passive systems, is probably to focus on those objects which are experiencing a transition in between the two phases. Among these, there are the so called E+A galaxies (Dressler & Gunn, 1983; Zabludoff et al., 1996), also named  $k+a$  and  $a+k$  (Dressler et al., 1999), or simply “post-starburst”. Their designation is derived from the characteristics in their spectra, which lack lines in emission and present strong Balmer absorption lines, typical of A-class stars (hence the “A” in their names), having a lifetime of some hundreds of Myr, up to about 1 Gyr. For this reason, such a spectral signature is very often used to identify a burst or an episode of enhanced star formation on those time scales.

The presence of strong hydrogen lines in absorption, and the concomitant absence of any emission line in the optical, can be easily achieved as the duration of the two phenomena producing them is different, with emission lines being typically produced from the intense ionizing continuum of very young (i.e. ages less than  $\sim 2 \times 10^7$  years) stars. Such a com-

ination can appear as the result of a star bursting episode being observed few tens of Myr after the star formation has stopped (e.g. Poggianti et al., 1999). Alternatively, a truncation in an otherwise continuous, regularly star forming pattern, might produce moderately strong Balmer absorption lines as well (e.g. Newberry et al., 1990; Leonardi & Rose, 1996).

Hence, in most cases, these are galaxies which have recently experienced a quenching of the star formation activity and are on their way to become passively evolving objects. Thus, despite the fact that they are quite rare if compared to the whole galactic population (see Quintero et al., 2004, and references therein), they may be one of the important keys to address galaxy evolution questions.

E+A galaxies were initially believed to be a prerogative of galaxy clusters, and a number of mechanisms have been proposed to explain their formation, including high speed galaxy-galaxy interactions (e.g. Zabludoff et al., 1996), mergers (Bekki et al., 2001), gas stripping by ram-pressure from the hot intracluster gas (Tonnesen et al., 2007; Ma et al., 2008). The latter in particular, detected in X-rays, is believed to be one of the main actors in a galaxy’s life, causing the quenching of the star formation in those systems which are accreting into clusters, through the efficient removal of their gas reservoirs.

Optical spectra contain the information we need in order to study, through the analysis of their integrated light, the stellar content of a galaxy: the stellar mass, the ages of stellar populations, their metallicity and the dust content are all characteristics that can, at least to some degree, be derived from such kind of data.

The WINGS<sup>1</sup> project (Fasano et al., 2006), and its spectroscopic follow-up (Cava et al., 2009), is providing the largest set of homogeneous spectroscopic data for galaxies belonging to nearby clusters. Spectral lines are of fundamental importance to characterize the stellar content and properties of a galaxy, providing also a quick and simple way to broadly classify them, according to their star formation history. The reader can refer to Poggianti et al. (1999) for an interpretation, from a theoretical point of view, of the meaning of the various spectroscopic classes.

In this paper we will describe the details of a method used to automatically measure the equivalent width (EW) of the most prominent spectral lines in WINGS optical spectra. The method, presented in Fritz et al. (2007) for the first time, is able to deal with spectra of low signal-to-noise, and provides a robust estimate of the uncertainty as well. We present and describe the catalogue of rest-frame EW, providing a spectral classification, and we compare the spectral properties of  $\sim 2000$  galaxies to other characteristics such as their luminosity, mass, morphology and to the environment where they reside.

The paper outline is as follows: we briefly present the dataset in Sect. 2 and explain and discuss the measurement method in Sect. 3. In Sect. 4 we point out some observational issues and describe the spectroscopic classification criteria, while in Sect. 5 we describe the properties of galaxies in our sample, based on their spectroscopic classification in relation with both other galaxies’ properties (such as luminosity, stellar mass, etc.) and with cluster’s properties

<sup>1</sup> You can refer to the WINGS website for a description of the project and updated details on the survey and its products: <http://web.oapd.inaf.it/wings/new/index.html>

as well. This is followed by a comparison with high redshift cluster galaxies (Sect. 6), and by a summary of our results (Sect. 7). Details on the EW catalog, together with an example, are given in Appendix A.

Throughout this paper we have adopted the usual convention of identifying emission lines with negative values of the EWs, and absorption lines with positive ones, with all the quantities given at restframe. Whenever stellar masses are used, we always refer to a [Salpeter \(1955\)](#) IMF, with masses in the  $0.15 - 120 M_{\odot}$  range, and stellar mass definition n.2, as discussed in [Longhetti & Saracco \(2009\)](#). Furthermore, we assume a standard  $\Lambda$  cold dark matter ( $\Lambda$ CDM) cosmology, with  $H_0 = 70$ ,  $\Omega_m = 0.3$  and  $\Omega_{\Lambda} = 0.7$ .

## 2. The dataset

Out of the 77 cluster fields imaged by the WINGS photometric survey (see [Varela et al., 2009](#), for the presentation of the photometric catalog), 48 were also followed-up spectroscopically. While the reader should refer to [Cava et al. \(2009\)](#) for a complete description of the spectroscopic sample, including data reduction, quality check, and completeness analysis, here we will briefly summarize the features that are more relevant for this work’s purposes. The results presented in this paper are based on WINGS spectra and catalogs discussed in [Cava et al. \(2009\)](#). Our apparent magnitude limit ( $V \sim 20$ ) is 1.5 to 2.0 mag deeper than the 2dFRS and SDSS surveys, respectively, and this is, in general, reflected in a higher mean number of member galaxies detected per cluster.

The target selection was based on the available WINGS optical B and V photometry ([Varela et al., 2009](#)), adopting a generous red cut well above the cluster red sequence. The aim of the selection strategy was to maximize the chances of observing galaxies at the cluster redshift without biasing the sample.

A good knowledge of the completeness level of the spectroscopic observations is required by the analysis that we will present, as this is a factor that must be accounted for in the derivation of luminosity functions, as well as anytime we want to use the spectroscopic sample to study magnitude-dependent properties (e.g. the different galaxy population fractions inside clusters, see [Poggianti et al. 2006](#)). We have computed both magnitude and geometrical (to account for the crowding of the fibers spectroscopy near the clusters’ centre) completeness which we describe in more detail in Appendix B.

Medium resolution spectra for  $\sim 6000$  galaxies were obtained during several runs at the William Herschel Telescope (WHT) and at the Anglo Australian Telescope (AAT) with multi-fiber spectrographs (WYFFOS and 2dF, respectively), yielding reliable redshift measurements. The fiber apertures were  $1''.6$  and  $2''$ , and the spectral resolution  $\sim 6$  and  $\sim 9 \text{ \AA}$  FWHM for WHT and AAT spectra, respectively. The wavelength coverage ranges from  $\sim 3590$  to  $\sim 6800 \text{ \AA}$  for the WHT observations, while spectra taken at the AAT cover the  $\sim 3600$  to  $\sim 8000 \text{ \AA}$  domain. Note also that, for just one observing run at WHT (during which 3 clusters were observed), due to a different setup, the spectral resolution was  $\sim 3 \text{ \AA}$  FWHM, with the spectral coverage ranging from  $\sim 3600$  to  $\sim 6890 \text{ \AA}$ .

The spectra were observed by adopting two configurations, depending on the galaxies’ flux: bright and faint (see

| LINE                   | $\lambda$ [ $\text{\AA}$ ] | EM/ABS | CRITERION                    |
|------------------------|----------------------------|--------|------------------------------|
| H $\alpha$ +NII        | 6563                       | E      | FIXED $\Delta\lambda$        |
| H $\alpha$             | 6563                       | A      | 1 <sup>st</sup> SLOPE CHANGE |
| Na (D)                 | 5893                       | A      | 1 <sup>st</sup> SLOPE CHANGE |
| Mg                     | 5177                       | A      | 1 <sup>st</sup> SLOPE CHANGE |
| [OIII]                 | 5007                       | A      | 1 <sup>st</sup> SLOPE CHANGE |
| H $\beta$              | 4861                       | E      | 1 <sup>st</sup> SLOPE CHANGE |
| H $\beta$              | 4861                       | A      | 1 <sup>st</sup> SLOPE CHANGE |
| H $\beta$              | 4861                       | E+A    | 2 <sup>nd</sup> SLOPE CHANGE |
| H $\gamma$             | 4341                       | E      | 1 <sup>st</sup> SLOPE CHANGE |
| H $\gamma$             | 4341                       | A      | 1 <sup>st</sup> SLOPE CHANGE |
| H $\gamma$             | 4341                       | E+A    | 2 <sup>nd</sup> SLOPE CHANGE |
| CO G-band              | 4305                       | A      | 1 <sup>st</sup> SLOPE CHANGE |
| H $\delta$             | 4101                       | E      | 1 <sup>st</sup> SLOPE CHANGE |
| H $\delta$             | 4101                       | A      | 1 <sup>st</sup> SLOPE CHANGE |
| H $\delta$             | 4101                       | E+A    | 2 <sup>nd</sup> SLOPE CHANGE |
| H $\epsilon$ +CaII (H) | 3969                       | E      | 1 <sup>st</sup> SLOPE CHANGE |
| H $\epsilon$ +CaII (H) | 3969                       | A      | 1 <sup>st</sup> SLOPE CHANGE |
| H $\epsilon$ +CaII (H) | 3969                       | E+A    | 2 <sup>nd</sup> SLOPE CHANGE |
| CaII (K)               | 3934                       | A      | 1 <sup>st</sup> SLOPE CHANGE |
| H $\zeta$              | 3889                       | E      | 1 <sup>st</sup> SLOPE CHANGE |
| H $\zeta$              | 3889                       | A      | 1 <sup>st</sup> SLOPE CHANGE |
| H $\zeta$              | 3889                       | E+A    | 2 <sup>nd</sup> SLOPE CHANGE |
| H $\eta$               | 3835                       | E      | 1 <sup>st</sup> SLOPE CHANGE |
| H $\theta$             | 3798                       | A      | 1 <sup>st</sup> SLOPE CHANGE |
| [OII]                  | 3727                       | E      | 1 <sup>st</sup> SLOPE CHANGE |

**Table 1.** The list of lines, whose equivalent width was measured, is reported here, together with their respective theoretical central  $\lambda$ . On the fourth column we report the adopted criteria for the determination of their underlying continuum (see details in Sect. 3), distinguishing, if needed, the occurrence of emission and/or absorption pattern (third column).

[Cava et al., 2009](#), for further details). In principle, an issue possibly affecting our observations, is the presence of saturated emission lines. While this would not be an issue for the spectral classification, it could indeed affect the lines’ flux measurements. However, saturation does not represent a relevant problem for our dataset, as spectra taken in the bright configuration are mostly luminous early-type galaxies, with no or at most faint emission lines. Spectra from the faint configuration, on the other side, belong to galaxies which are not bright enough to display saturated emission lines.

## 3. The method

Given the rather large number of spectra in the WINGS spectroscopic sample, we developed an automatic method capable of yielding accurate measurements of the most important spectral lines. In table 1 we list the 14 lines that are measured for each spectrum.

Some automatic measurement procedures are already available in the literature (such as ARES, [Sousa et al. 2007](#), DAOSPEC, [Stetson & Pancino 2008](#), PACCE, [Riffel & Borges Vale 2011](#) or, more recently, TAME by [Kang & Lee 2012](#)). While in general they are mainly focused on the measurement of absorption lines, and in spectra with a high S/N, we would ideally like to be able to use the information from spectra where the lines are still detectable even though somehow affected by the noise. For example,

as Goto et al. (2003) noted, an EW value derived by means of a Gaussian fit to the line, yields reliable results only in high S/N spectra, unless the fit is performed interactively. Furthermore, we are also interested in emission lines and in the “mixed” case, in which absorption and emission profiles overlap.

When measuring an EW in a spectrum, the choice of the continuum turns out to be a critical issue. In general, one would require that the line profile is fully included, and that the measurement is made without being affected by other lines in the proximity, or by noisy features such as spikes, which could dramatically change the continuum level, and hence the EW value. Defining the line profile by adopting a fixed wavelength range, centered on the theoretical wavelength characterizing each line, can be an unreliable choice because: 1) the line width can depend on the EW itself (being larger as its value increases) or on the galactic kinematic and 2) on a blind-measure approach, it is not possible to verify whether the noise is dominating both the line and the continuum level. The method we adopted for the lines measurements has already been described in Fritz et al. (2007), where we have preliminarily used it to constrain the lines’ intensity on a theoretical spectral model. Here we will recall the most salient features and go into a more detailed description.

The algorithm measures the equivalent width of a line, no matter if in absorption, emission, or including both components, by choosing the appropriate value of the Full Width at Zero Intensity  $-\Delta\lambda$  which is symmetric with respect to the nominal (theoretical) line’s centre (see table 1). As we show in Fig. 1, the edges of this interval are used to define both the spectral continuum (red markers at the extremes of the green-dashed line) and the range over which the line is measured. The spectral continuum is approximated by a straight line –green-dashed in Fig 1– and the EW value is found by summing the dashed areas, divided by the average continuum value.

To find the proper EW value, the line is first measured over a very short interval  $\Delta\lambda$ , under-sampling the real value; then, various values of the EW are computed as a function of  $\Delta\lambda$ , which is increased at steps of 1 Å, starting from an initial width of 4 to 8 Å, depending on which line is measured, up to  $\sim 80$  Å. The upper panel of Fig. 2 illustrates this process. Here the red straight lines represent the continuum level defined over increasingly larger values of  $\Delta\lambda$ , and the dashed regions represent the area where the spectral line is measured (and whose profile is highlighted with a blue line).

The correct value of the EW is found, among those measured in this way, by analysing the EW trend curve (see Fig. 2, lower panel). In fact, the absolute value of the EW will, in general, monotonically increase as the  $\Delta\lambda$  increases, since the line profile is increasingly better sampled. The point where the trend curve has its first change in slope (first derivative equal to zero), is generally where the line should ideally be measured, both for emission and absorption lines. In spectra with high Signal-to-Noise (S/N, hereafter), or in theoretical SSPs spectra, an asymptotic behaviour of the trend curve is also providing the correct EW value. An important exception is the case of an absorption + emission profile, which can be easily found in lines such as H $\beta$ , H $\gamma$  or in some cases even in the higher order lines. In this case, the first change in the slope of the trend curve will happen in correspondence to the change from sampling the emis-

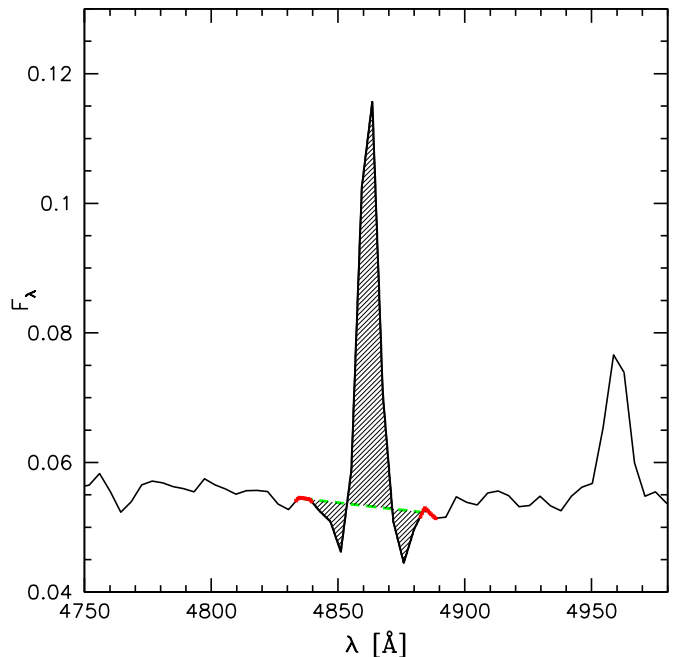


**Fig. 1.** Here we show how we define the areas that are used to compute an equivalent width. In this example we plot an H $\beta$  profile which includes both an absorption and an emission component. The green-dashed line is meant to approximate the spectral continuum while its length,  $\Delta\lambda$ , is used also to define the wavelength range over which the line itself is measured.

sion and the absorption profile. When this is the case, the second change in slope identifies the correct EW value (see Fig. 2, where such an example is given).

Hence, in order to recognise the absorption+emission pattern, it is first checked whether the EW trend curve starts with negative or positive values, for those lines that can be both measured in absorption and emission (hydrogen lines). If small values of  $\Delta\lambda$  yield negative EW, then we are very likely in the presence of an emission+absorption pattern, and the EW determination is treated accordingly.

The H $\alpha$  line is treated in a different way: due to the close proximity of the two Nitrogen forbidden lines ( $\lambda = 6548$  and  $6584$  Å, respectively), when the line is in emission the trend curve analysis may become too complicated and impossible to treat with this method. This is particularly true in a number of different, various situations such as when the lines are very bright, or if the gas emitting the lines has multiple velocities components, so that the three lines’ profile can be partially blended, but also for medium resolution spectra, like the ones we are dealing with. To properly deal with such issue, we first measure the line within a small ( $\sim 15$  Å)  $\Delta\lambda$  interval; in this way we check whether the line is in absorption or in emission. In the first case, the trend curve analysis method is applied, as for the other lines. In the second case, a fixed  $\Delta\lambda \sim 70$  Å is adopted, so that this measure will safely include both H $\alpha$  and the two Nitrogen lines.

We stress here that this method has been tweaked in order to deal with spectra dominated by an emission component of stellar origin. Of course, we can also properly measure lines in LINERS or type-2 AGN, at least for the

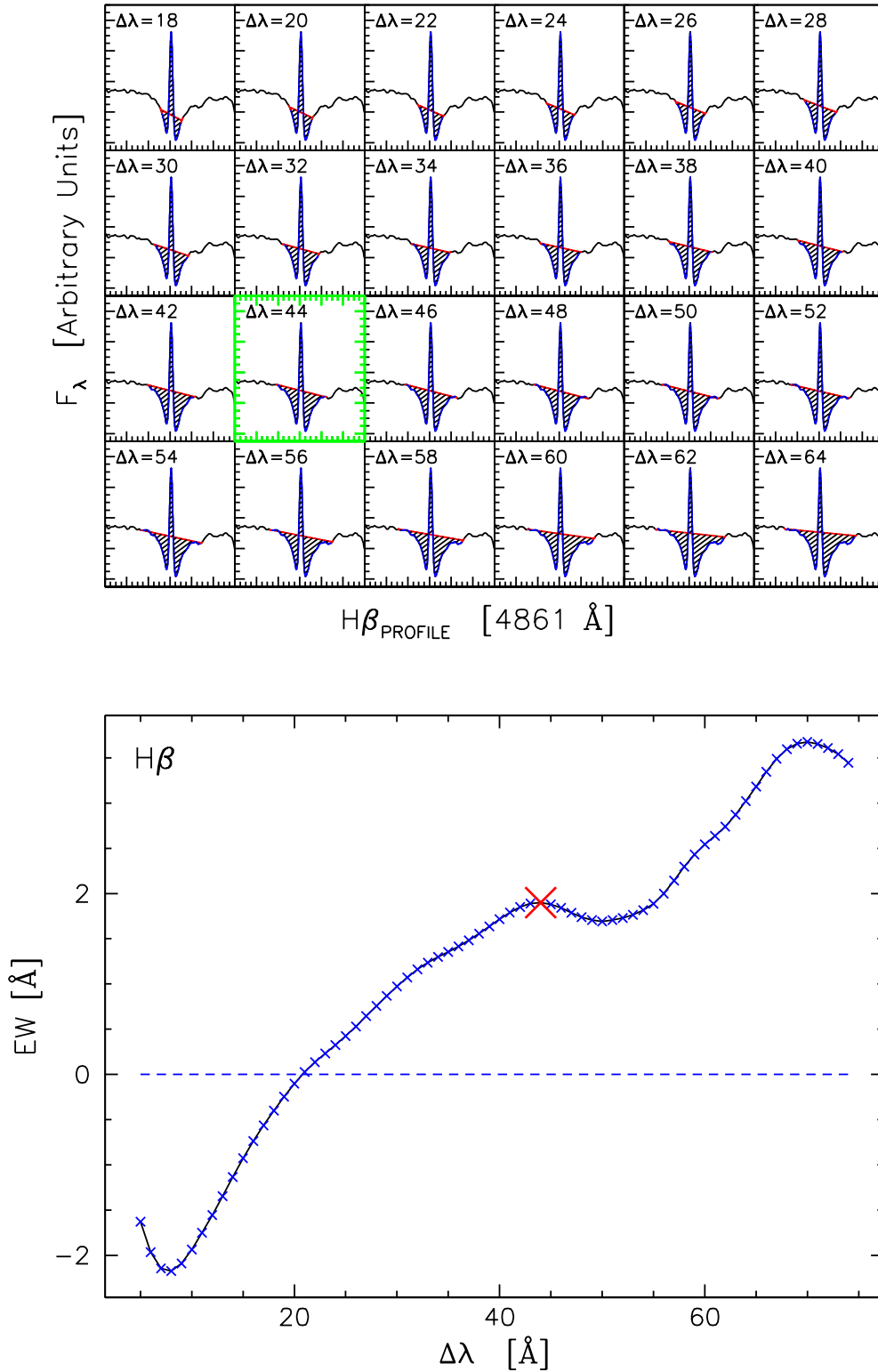


**Fig. 2.** Here we visually illustrate how our EW measurement method works on an observed H $\beta$  line: in the *upper panel* we show how the EW is iteratively measured at increasingly larger  $\Delta\lambda$  (red, straight line) which are also used to define the continuum level. The dashed regions correspond to the area measured for the EW determination. The analysis of the EW trend curve, plotted on the *lower panel*, provides the correct observed value, shown by the red cross. In this case, in which both emission and absorption components are present, it corresponds to the second zero of the first derivative of the trend curve itself.

few ones found in WINGS (an adjustment to the maximum value of the EW might be needed to deal with the high-luminosity ones). The measurements of (emission) lines in type-1 AGN is instead a much more complicated issue, as in that case permitted lines can have FWHM of several thousands of km/s, and they easily end up blending with neighbouring ones (e.g.  $H\beta + [OIII]$ ). Our method is currently not capable of properly measuring lines in such spectra, which are anyway extremely rare in our sample, hence not affecting by any meaning the scientific analysis.

In Table 1 we summarize the rules used for the choice of the most appropriate value of  $\Delta\lambda$ . In general, when only one of the profiles (i.e. emission or absorption) is present, the first change in the slope of the EW trend curve represents the best guess for the continuum determination. If both the emission and absorption components are instead present, the  $\Delta\lambda$  corresponding to the second slope change is instead chosen.

We have chosen a sample of spectra of different types, spanning from early to late-type, and with different signal-to-noise, and we have measured, using the package `splot` within IRAF, the equivalent widths of the most significant lines. The comparison between the automatic and the manual methods are shown, for a subsample of 4 lines, in Fig.3 of Fritz et al. (2007), but the results are very similar for the other lines. In summary, we found that our automatic method returns EW values which are in agreement, within the estimated errorbars, with those that have been manually measured. Furthermore, the detection of emission lines is reliable for observed spectra with a signal-to-noise values down to  $\sim 5$ . Some subjectivity can, of course, affect the choice of the underlying continuum especially in spectra with the lowest quality, but this is then reflected in a larger errorbar.

### 3.1. Uncertainties

To give an estimate of the errorbars associated with an EW measurement is not straightforward. We consider the main source of uncertainty to be the choice of the continuum. As already pointed out, the EW measurement is quite dependent on the fluctuations of the nearby continuum, hence, on the local S/N. To account for this, we measure the equivalent width of the line at a  $\Delta\lambda$  that is, respectively,  $5 \text{ \AA}$  (this number being defined empirically, by checking the lines' measurements on observed spectra at different S/N) larger and smaller than the value found by the automatic tool, and take the semi-difference of these two values as the errorbar. Note that, by adopting such a definition for the uncertainties on the definition of the spectral continuum, the better the latter is defined, the smaller the measured uncertainty will be. Even though this is the dominant source of uncertainty, we also account for a ‘‘poissonian’’ error, given by:

$$\Delta(EW) = 0.5 \times \sqrt{|EW|} \quad (1)$$

which is added in quadrature to the measurement uncertainty. Errorbars computed in this way are in very good agreement with those formally computed by propagating the measured errors.

As a further check, we have used the subsample of SDSS galaxies with spectroscopic data which are in common with our survey (see also the comparison performed in Fritz et

al., 2011) to compare the EW values and see whether they agree within the uncertainties calculated by the measurement method. Of the 395 objects with spectroscopic data from both surveys we use, for this comparison, the  $\sim 250$  which are brighter than  $M_V = -18$  (see Sect.4.2). Before proceeding, an important caveat must be considered: there is a difference in the size of the fibers used in taking WINGS and SDSS' data, and this means that the physical regions we are observing might include, in some cases, slightly different stellar populations. Added to this, the location of the fiber might also not be exactly the same and the signal-to-noise of some of the spectra can also be very different. All these effects might increase the scatter in the comparison.

Despite this, we find that the EW values measured for the two different datasets, and in particular those of  $[OII]$  and  $H\delta$  (which are those upon which our classification scheme is based), very well agree within the given uncertainties. The rms of the relation comparing  $[OII]$  measurements is  $\sim 6 \text{ \AA}$ , which is in fair agreement with the average errorbar of  $\sim 4 \text{ \AA}$ , especially if we take into account the aforementioned caveats on the fibers size and position. In the case of  $H\delta$ , the rms is  $\sim 0.8$  which again is consistent with the average errorbar of  $\sim 0.7 \text{ \AA}$ . This not only makes us more confident that the EW uncertainties are well estimated, but it further strengthens the reliability of the spectral classification.

### 3.2. Noisy detections and caveats

One of the trickiest issues concerns the detection of lines in spectral regions with low S/N or in the proximity of the telluric absorption bands which are sometimes not properly subtracted from the spectra. First of all, we do not want the measurements, i.e. the analysis of the EW trend curve, to be influenced by the fluctuations produced by noise and, second, we require that noise fluctuations and spikes are not interpreted as real spectral lines. The blue range of a spectrum contains, for typical WINGS spectra and redshifts, 7 relevant lines within a  $400 \text{ \AA}$  range and, unfortunately, is also the most prone to flux calibration uncertainties and the most affected by noise. To overcome this issue, some empirical criteria are defined to recognise noisy patterns and to distinguish them from real spectral lines:

- the EW of forbidden lines can only be negative (i.e. in emission); positive values are hence interpreted as the line being absent or the spectrum highly noisy in that region;
- late Balmer lines, such as  $H\delta$  or  $He$ , can be measured in emission if and only if other lines –such as for example,  $[OII]$ ,  $[OIII]$ ,  $H\beta$  or  $H\alpha$  which are typically brighter– are also detected in emission;
- an upper limit is set to the values of both absorption and emission lines: EWs of absorption lines cannot be higher than  $16 \text{ \AA}$ , a value derived from SSP models. When emission lines are taken into account, the maximum (absolute) value that a line can assume is dependent on the line itself, and was computed from SSP spectra. Lines having EW outside these ranges are considered as noise.

The shape and, more in general, the characteristics of the EW trend curve can depend on the spectral resolution. In fact, especially in low signal-to-noise and high resolution

spectra, the trend curve can assume an erratic behaviour, particularly at a local level. Thus, the method had to be slightly tweaked so to take into account for a possible sensitivity to the spectral resolution. This was done by testing and calibrating the algorithm on spectra having the same resolution of those in the WINGS datasets. Furthermore, as described in §3.1, we have applied our method to a set of SDSS spectra, and found that it does not show a strong sensitivity on the resolution, at least as far as datasets with such characteristics are considered.

Finally, we consider as unreliable values above  $-2 \text{ \AA}$  for the EW of [OII] and [OIII]. These cases are identified with a 0.0 in the catalogs.

#### 4. WINGS spectra

The WINGS spectroscopic sample was built up from two sets of observations: spectra of galaxies in clusters at a negative declinations were taken with the 2dF multifiber spectrograph at the Anglo-Australian Telescope, and constitute the “south sample”. Spectra in the “north sample” were instead taken at the William Herschel Telescope using the AF2/WYFFOS (see §2 for more detailed information about the spectra).

Due to both technical issues and bad weather conditions, a number of spectra taken at the William Herschel Telescope turned out to be of very poor quality, and had to be discarded as not suitable for our work. In this way, the number of spectra of members for some clusters had been so drastically reduced, that we decided not to include these clusters in our analysis. In Appendix C we provide more details both on the issues and on the adopted rejection/acceptance criteria.

This selection reduces the number of spectra that are used in this work to 4381 out of the  $\sim 6000$  that were originally observed, of which 2744 are spectroscopically confirmed members, belonging to 29 clusters in both the south and north sample. In Table 2 we report the cluster names, the total number of spectra and the confirmed members, and their redshifts.

##### 4.1. Spectral classification

Adopting the spectral classification defined by Dressler et al. (1999) (MORPHS collaboration), which was developed to study distant galaxy clusters, we divide the spectra of our sample into 6 classes, based on the EW of [OII] and  $H\delta$ , according to the scheme presented in Table 3. Spectra for which none of the two lines was detected are classified as *noisy*. The broad physical meaning of such a classification is discussed in detail by Poggianti et al. (1999) and Poggianti et al. (2009b); we summarize it briefly in the following:

- *e(a)* emission-line spectra with strong  $H\delta$  in absorption, signature of the presence of A-type stars. They are typical either of dusty starbursts, or of systems where an episode of substantial star formation was abruptly interrupted, and only a residual activity might be currently present;
- *e(b)* emission-line spectra with very strong emission lines, typical of star-bursting systems with low to moderate dust extinction;
- *e(c)* emission-line spectra with moderate-to-weak emission and moderate-to-weak  $H\delta$  in absorption, typical of

| CLUSTER | TOTAL | MEMBERS | REDSHIFT |
|---------|-------|---------|----------|
| A1069   | 97    | 39      | 0.0653   |
| A119    | 241   | 156     | 0.0444   |
| A151    | 235   | 85      | 0.0532   |
| A1631a  | 184   | 109     | 0.0461   |
| A1644   | 225   | 165     | 0.0467   |
| A2382   | 209   | 134     | 0.0641   |
| A2399   | 191   | 110     | 0.0578   |
| A2415   | 180   | 95      | 0.0575   |
| A3128   | 274   | 196     | 0.0600   |
| A3158   | 263   | 172     | 0.0593   |
| A3266   | 247   | 215     | 0.0593   |
| A3376   | 130   | 86      | 0.0461   |
| A3395   | 178   | 121     | 0.0500   |
| A3490   | 186   | 69      | 0.0688   |
| A3497   | 135   | 74      | 0.0680   |
| A3556   | 155   | 105     | 0.0479   |
| A3560   | 156   | 107     | 0.0489   |
| A3809   | 165   | 95      | 0.0627   |
| A500    | 133   | 89      | 0.0678   |
| A754    | 141   | 119     | 0.0547   |
| A957x   | 116   | 62      | 0.0451   |
| A970    | 172   | 114     | 0.0591   |
| A1795   | 57    | 29      | 0.0633   |
| A1983   | 66    | 31      | 0.0447   |
| A2457   | 50    | 35      | 0.0584   |
| A2626   | 41    | 27      | 0.0548   |
| A376    | 58    | 43      | 0.0476   |
| Z8338   | 60    | 37      | 0.0494   |
| Z8852   | 36    | 25      | 0.0408   |
| TOTAL   | 4381  | 2744    |          |

**Table 2.** List of the clusters used for this work. For each cluster we report the total number of spectra for which we have reliable EW measurements, those which are confirmed cluster members, and the cluster’s redshift.

a regular (non-starbursting) star formation pattern, as those distinctive of “normal” spiral galaxies;

- *k* spectra resembling those of K-type stars, lacking emission lines and with weak  $H\delta$  in absorption, typical of passively evolving galaxies with neither current nor recent star formation activity. Such spectra are normally found in elliptical galaxies;
- *k+a/a+k* spectra displaying a combination of signatures typical of both K and A-type stars, with strong  $H\delta$  in absorption and no emission lines, typical of post-starburst/post-starforming galaxies whose star formation was suddenly truncated at some point during the last 0.5 – 1 Gyr.

Following this broad classification, all emission lines galaxies are those which are undergoing a process of star formation at the very moment of their observation. Another origin of emission lines is also possible and it will be discussed later on. The other types represent “passive” spectra, the *k* being dominated by old stars (older than  $\sim 2$  Gyr), and the *k+a* and *a+k* showing evidence for an increasingly important presence of A-class stars, which are commonly recognised as a signature of a relatively recent ( $< 1$  Gyr) burst or at least activity of star formation.

Note that in few cases, in order to distinguish between the 3 emission line classes, we used, if possible, also  $H\beta$  and [OIII]. These two lines were used in those cases, mostly for spectra of the north sample, for which the [OII] line either was out of the observed range, or it was non-detected (the

| SP.TY. | cat ID | [OII]    |     | H $\beta$  |     | [OIII] |     | H $\delta$ | N (%)  |
|--------|--------|----------|-----|------------|-----|--------|-----|------------|--------|
| e(a)   | 1      | < 0      | OR  | < 0        | OR  | < 0    | AND | $\geq 4$   | 6.9 %  |
| e(b)   | 2      | < -40    | OR  | < -12.5    |     | ...    | AND | < 4        | 2.5 %  |
| e(c)   | 3      | -40 to 0 | OR  | -12.5 to 0 | OR  | < 0    | AND | < 4        | 29.9 % |
| k      | 4      | > 0      | ... | ...        | ... | ...    | AND | < 3        | 49.6 % |
| k+a    | 5      | > 0      | ... | ...        | ... | ...    | AND | 3 to 8     | 10.4 % |
| a+k    | 6      | > 0      | ... | ...        | ... | ...    | AND | $\geq 8$   | 0.7 %  |

**Table 3.** Summary of the criteria adopted to classify the spectra based on spectral lines criteria. Other lines (namely H $\beta$  and [OIII]) were introduced with respect to previous works, in order to be able to classify a spectra in those cases when the [OII] line was out of the observed spectral range or overwhelmed by noise. The last column presents the spectral type fractions, corrected for incompleteness, among galaxies to which a spectral classification could be assigned.

blue range of the spectra is often quite noisy). The use of H $\beta$  in particular, has been already exploited by Yan et al. (2006) as a mean to distinguish and properly classify  $e(a)$  and  $k+a$  spectra. We searched for a relation between either the EW of [OIII] (5007 Å), which is easily detected –when present–, or that of H $\beta$ , and the EW of the [OII]. This relation is intended to be used only to distinguish between the  $e(b)$  ([OII] < -40 Å) and the  $e(c)$  ([OII]  $\geq$  -40 Å) classes, while the classification as an  $e(a)$  is made mainly by means of H $\delta$ .

No clear trend is found for either of the two lines and, if we average the EW value of [OIII] and H $\beta$ , for those galaxies where  $\text{EW}([\text{OII}]) \leq -40$ , we obtain -12.5 and -32.5 Å, for H $\beta$  and [OIII], respectively. We choose to use H $\beta$ , as a proxy for the [OII] line, since it has the lower dispersion (even though we are conscious that this is in part due to the fact that also the average value of H $\beta$  EW is lower with respect to that of [OIII]). Table 3 is meant to summarize the criteria used to assign the spectral classification.

Note that the spectrographs at both telescopes allow us to observe, for all WINGS clusters, the spectral region containing the [OII] line, which is crucial for the classification scheme we have chosen. In the worse case, at the cluster’s average redshift, the [OII] line is observed at  $\sim 3880$  Å, well above the lower limit of 3600 Å. On the other side, most of the spectra in the north sample do not encompass the H $\alpha$  line which is anyway not used for spectral classification purposes, hence not affecting any of the derived quantity we use for the present work.

#### 4.2. Compatibility between south and north sample classification

The V-band absolute magnitude distributions are shown in Fig. 3, for the north and south samples separately, distinguishing also the spectroscopically confirmed members. Absolute magnitudes used for this work are those computed based on the best-fit model to the observed spectrum (see Fritz et al., 2011), so that the  $k$ -correction is automatically taken into account, and no assumptions need to be made. We note that at the faint end the north distribution declines at magnitudes brighter than the south sample ( $M_V \simeq -18.5$ ), probably due to severe incompleteness setting in at brighter magnitudes in the north. Nevertheless, as the north subsample contains less than 10% of the total WINGS members, this will not alter the significance of our results. For these reasons, we can carry on our analysis of the whole sample using galaxies with  $M_V < -18$ .

In Fig. 4 we show the distribution of the various classes within the north and south subsamples for member galax-

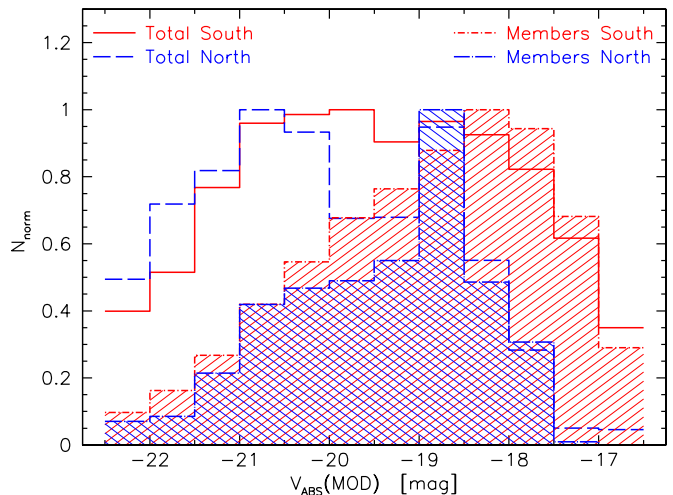


**Fig. 3.** Distributions of absolute V magnitude for galaxies in the north and south samples (different colors and lines). Absolute magnitudes are computed as the integral convolution between the rest-frame model spectrum and the V band transmission curve. All distributions are normalised to their peak number, and both magnitude and geometrical completenesses are taken into account.

ies. Following what was previously discussed, a cut in absolute magnitude at  $M_V = -18$  was applied. We choose to show only cluster members, since the non-members population contains a mix of field galaxies and foreground structures, which we are not able to properly distinguish. The percentage of the various classes are computed taking into account both magnitude and geometric completeness.

As described in Appendix C, the EW measurements had to be performed manually for some spectra, and this could, at least in principle, make the measures –and hence the classification– non homogeneous between the south and north subsample, possibly introducing some bias.

From Fig. 4 we note that the relative number of the various spectral types is similar in the two samples, meaning that, once completeness corrections are taken into account, and as long as galaxies brighter than  $M_V = -18$  are considered, the two samples can be considered as homogeneous and comparable, within the statistical uncertainties.

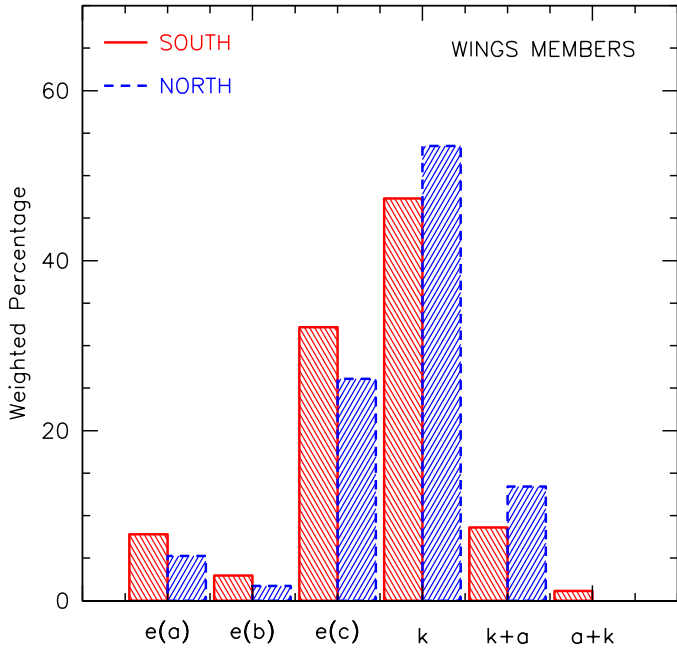


**Fig. 4.** Spectral types distribution of WINGS spectroscopically confirmed members. South and north samples are shown separately with different colours and lines, for comparison. A cut at absolute magnitude  $M_V = -18$  has been applied.

## 5. The characteristics of the local clusters galaxy population

We now analyse the properties of the galaxies in our sample, with a focus on their spectral classification and related characteristics.

### 5.1. General properties

We were able to successfully classify about 90% of the spectra of our survey (both cluster members and background objects), based on [OII] and H $\delta$  (or H $\beta$ , when the [OII] lines was not observed, see Sect. 4.1). Spectra without a classification either have a very low S/N, or the lines were not measured due to strong artifacts affecting their profiles.

With this information, we can now analyse the properties of the cluster population, discussing the characteristics of the various spectral types as a function of their physical properties such as luminosity, morphology, stellar mass, and position within the cluster. To properly do this, we limit our sample so that it includes only galaxies with a total absolute magnitude equal or brighter than  $-18$  in the V band (see Sect. 4.2). With this cut in magnitude, we are left with 2296 out of the original 2744 in the members' sample. From now on we will consider only objects in this magnitude limited sample, unless otherwise stated. We stress here that at this magnitude limit the south sample is complete at the  $\sim 70\%$  level (see the discussion in Cava et al., 2009).

Table 4 summarizes the number distribution of the three main morphological types. Galaxy morphologies are taken from Fasano et al. (2012) and have been obtained with MORPHOT, an automated tool designed

| TOTAL | ELLIPTICALS | S0    | SPIRALS |
|-------|-------------|-------|---------|
| 2296  | 653         | 1052  | 574     |
| ...   | 28.4%       | 45.8% | 25.0%   |

**Table 4.** Summary of all the morphological types, identified as cluster members, in our magnitude limited sample (corrections for incompleteness are here not taken into account). BCGs are not included.

to simulate as closely as possible a visual morphological classification. MORPHOT uses a combination of 21 imaging parameters complementing the classical Concentration/Asymmetry/clumpiness indicators, derived from the V-band WINGS images, and provides a parametrical morphological classification based both on a maximum likelihood technique and on a neural network machine (see Fasano et al., 2012, for details). This piece of information will be used later on (see, e.g., Sect. 5.3).

Considering the spectral classification as outlined in Sec. 4.1, we found that the galaxy population in local clusters is dominated by the  $k$  spectral type, including about 50% of the galaxies in our spectral sample, followed by the  $e(c)$  class ( $\sim 30\%$ ). The post-starburst classes ( $k+a$  and  $a+k$ ) represent about 11% of all the galaxies while the two other emission-lines classes,  $e(a)$  and  $e(b)$ , contain 7 and 3% of all members, respectively (see Table 3). These fractions have been calculated taking into account completeness corrections.

### 5.2. The V-band luminosity distribution

On the left panel of Fig. 5, we compare the distributions of the V-band absolute magnitude for the various spectral classes. Note that this magnitude was computed from the best fit model to the observed spectrum (see Fritz et al., 2007, 2011).

The V-band luminosity distributions span a range of 3 to 5 magnitudes, depending on the spectral type, peaking in general at different magnitudes and displaying also a different median luminosity as a function of the spectral class.

It shows no significant differences between the  $e(a)$  and the  $e(b)$  spectral classes, peaking around  $M_V \sim -18$  for both types, having the same median luminosity and very similar range. The luminosity function for the other emission-line type, the  $e(c)$  galaxies, substantially differs in that not only it displays a tail towards brighter magnitudes, but it also peaks at higher luminosities ( $M_V \sim -19$ ; note this is above the magnitude limit we consider).

As for the distributions of the two post-starburst classes  $k+a$  and  $a+k$ , they both peak around  $M_V \sim -18$ , even though, especially in the case of the  $a+k$  class we are most likely limited by the poor statistics. They differ, though, with respect to the range in luminosity which is broader for the  $k+a$  class, reaching  $M_V \sim -22$ , almost matching the high-luminosity tail seen for the  $e(c)$  and  $k$  galaxies. The characteristics of the luminosity distribution we find for  $k+a$ 's, are very similar to those of the ones in the local, massive Coma cluster (see Poggianti et al., 2004), lacking a significant bright population, and having a similar typical absolute magnitude of  $\sim -18$ .

The V-band luminosity distribution of galaxies with a  $k$ -like spectrum is yet clearly different with respect to all the

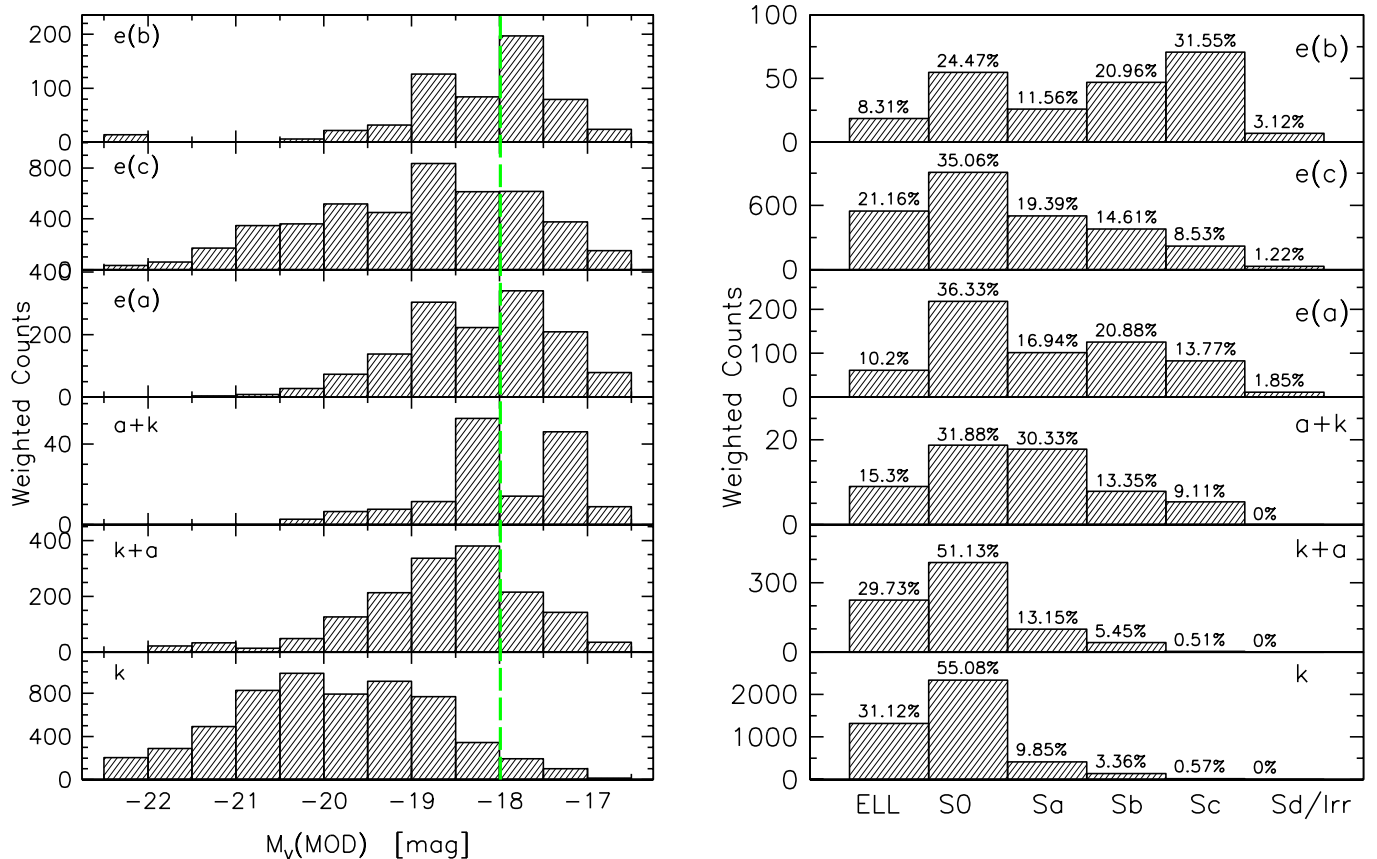


**Fig. 5.** *Left panel:* shaded histograms represent the number of galaxies in the 6 spectral types, as a function of the absolute V magnitude; the green-dashed line marks the magnitude limit of the subsample used in the analysis (for this plot only, we consider no cut in magnitude). Galaxies brighter than  $M_V = -22.5$  are included in the brightest bin. *Right panel:* occurrence of morphological types as a function of the spectral class. The percentages refer to the number of objects with a given morphology with respect to each spectroscopic class. For both plots data have been weighted by both magnitude and geometric completeness. For the right-hand plot only galaxies with  $M_V < -18$  have been considered.

other classes in basically all of its characteristics: peaking at  $M_V \sim -20.5$ , they also have the most luminous tail in the distribution while at the same time lacking, when compared to the other classes, a significant population of objects with absolute magnitudes lower than  $M_V \sim -19$ . In fact, together with the  $e(c)$  type, this is the only class whose luminosity function decreases before our magnitude limit cut.

### 5.3. Morphology distribution of the spectral types

An analysis of the morphological mix of the WINGS galaxy population has already been carried out in Poggianti et al. (2009a). Here we focus on the relation between morphology and spectral type.

In the right-hand panel of Fig.5 we show how the spectral classification correlates with the morphology for our magnitude-limited sample. WINGS galaxies follow in general the broad relation between morphology and star formation history.

Globally, the dominant morphological type is represented by S0s, accounting for more than 50% of both the passive spectral type  $k$  and the post-starburst  $k+a$ . They are also the most numerous among every spectral class with

the exception of the  $e(b)$ , which is instead dominated by late-type spirals (Sc). More than 80% of the passive galaxies  $k$  are early-types (E+S0), and the same goes for the post-star forming  $k+a$  class.

On the other side, the majority of  $e(a)$ ,  $e(b)$  and  $a+k$  are spirals. While the morphological fractions of  $e(a)$  and  $a+k$  are similar, the  $e(b)$  class clearly stands out being dominated by spiral galaxies, with more than the 50% of objects being found among later types than Sb. The  $e(c)$  spectral type is almost equally populated by early (E+S0) and late types (Sp).

The presence of the various morphological types among the  $k$  and  $k+a$  galaxies is very similar: we observe a clear prevalence of ellipticals and S0s, no Sd/Irregular, and a fraction of spirals less than 20% in both classes. Furthermore, this fraction is monotonically decreasing when going from  $a+k$ , to  $k+a$  and finally to  $k$ , where the relative occurrence of Spiral galaxies is the lowest, probably mirroring the transition from a post-star forming phase to a passive evolution pattern.

Finally, there seems to be a significant difference in the morphology distribution between the two so-called post-starburst classes,  $k+a$  and  $a+k$ , with the latter distribution resembling more that of the spiral types (even though it

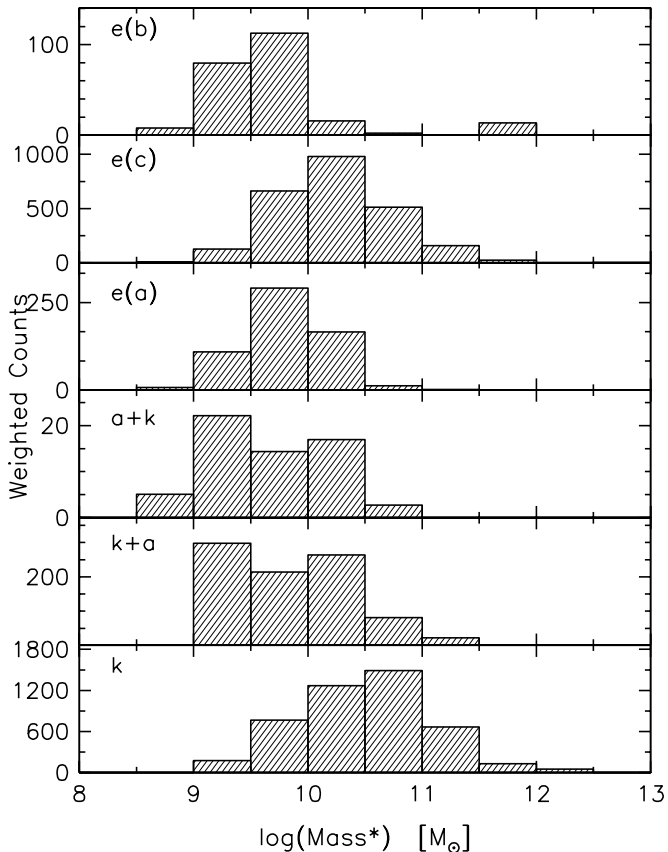


**Fig. 6.** Stellar mass distribution for the 6 spectral types, in the magnitude limited sample, and for objects within  $R_{500}$ .

should be pointed out that the statistic is not optimal for the  $a+k$  class). A similar result was found by Dressler et al. (1999) at higher redshift.

To summarize, while there is indeed a broad correspondence between the morphological and spectral classifications, we find that galaxies in local clusters lack an *univocal* equivalence between their morphology and their spectral characteristics, a result already well known at high redshift (e.g. Dressler et al., 1999; Couch et al., 2001), meaning that the evolution of these two properties is, at least to some degree, decoupled.

#### 5.4. Emission line galaxies in local clusters

As already described in Sect. 5.2, the V-band luminosity distribution is very similar for the  $e(a)$  and  $e(b)$  spectral type, but substantially different for the  $e(c)$ . This somehow reflects on the stellar mass distribution (see Fig. 6; mass values are taken from the catalog presented in Fritz et al., 2011):  $e(c)$  galaxies peak at around  $10^{10.5} M_{\odot}$ , while the distribution for  $e(a)$  and  $e(b)$  peaks at stellar mass values 0.5 dex lower, with the  $e(a)$  population having, in proportion, a slightly higher fraction of massive galaxies with respect to the  $e(b)$ 's; otherwise the distributions of the latter two spectral types are very similar.

It should be said that, as we noted in Fritz et al. (2007), the more a galaxy has been actively forming stars in a recent past, the more difficult it is to have a robust estimate

of the stellar mass of the oldest stars from optical spectra alone, given their high mass-to-light ratios. Thus, in principle, the mass of  $e(b)$  galaxies is the one potentially more prone to be underestimated when calculated with data similar to ours. Nevertheless, a comparison with an estimate of the stellar mass calculated using only B and V-band photometry and adopting the Bell & de Jong (2001) recipe, gives fully compatible results, (see Fritz et al., 2011). A similar check exploiting K-band photometry from Valentinuzzi et al. (2009), further validates our results.

We now analyse the fraction of star-forming galaxies as a function of the cluster properties, such as its velocity dispersion and X-ray luminosity. As done in several previous works (see e.g., Dressler et al., 1999; Poggianti et al., 2006), we use the [OII] (3727 Å) as a tracer for the star formation activity, so to be able to consistently compare our results with other studies, especially those at higher redshift. Even though this line is prone to reddening issues and its intensity depends on both the gas metallicity and physical conditions, its presence/absence can be reliably used to discriminate between star-forming/passively evolving galaxies.

For each cluster we calculate the fractions of galaxies, weighted for completeness, displaying the [OII] line in emission, i.e. having a rest-frame EW  $< -2$  Å. As the data coverage, in terms of projected radial distance, is limited by the characteristics of the spectrographs we have used for the survey, and since the clusters span a non negligible range in redshifts, observing galaxies in clusters at different distances means we are sampling areas at different distances from the cluster's centre. For this reason, in order not to introduce any bias and sample the galaxy population homogeneously, only galaxies within  $R_{500}$  (we use the relation  $R_{500} \simeq 0.50 \times R_{200}$ ) are considered.

The results are then plotted against the two main global properties of the clusters, namely their velocity dispersion and X-ray luminosities, and displayed in Fig. 7.

In Poggianti et al. (2009a) we have already analysed the frequency of morphological types as a function of the cluster velocity dispersion and X-ray luminosity. Here we perform a similar analysis based on the spectral classification, where X-ray luminosity ( $L_X$ ) and the cluster velocity dispersion ( $\sigma$ ) are used as a proxy of the total cluster mass.

Similar to what found in Poggianti et al. (2009a) we note that there is no, or at most a weak correlation between the fraction of galaxies with emission lines and the velocity dispersion, as far as clusters having a velocity dispersion in the  $\sim 500 \div 1400$  km/s range are concerned (i.e. the range of WINGS clusters). This is also in agreement with the results of Poggianti et al. (2006), who analysed a low-z galaxy cluster sample drawn from the SDSS. This result suggests that the global properties of a cluster are not the main physical drivers of the build up of the mixture of spectral types. A similar result is found also for post-starburst galaxies (see Sect. 5.5).

We checked with a Spearman test whether there is any significant correlation between the emission line fraction and the X-ray luminosity. The test yielded a correlation coefficient of 0.26, which indicates that there is none.

The fraction of star-forming galaxies in WINGS clusters, calculated from each single cluster, is  $\sim 33 \pm 10\%$ , with a large scatter at any given  $\sigma$  and  $L_X$ . This fraction is larger than the 23% found in Poggianti et al. (2006), but this is

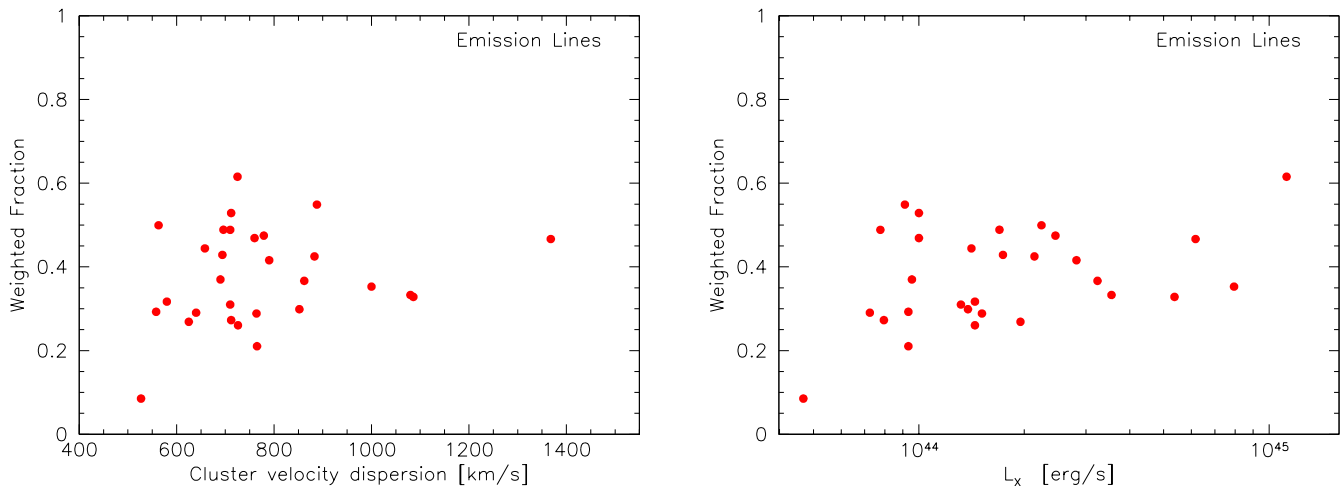


**Fig. 7.** Fraction of emission line galaxies (i.e. belonging to any of the first three spectral classes defined in Table 3) as a function of the cluster velocity dispersion (*left*) and total X-ray luminosity (*right*). Only galaxies within  $R_{500}$  are taken into account (see text for details).

likely due to the differences in the magnitude limit in these two studies, being deeper in WINGS, and the different limit for [OII] detection ( $-3 \text{ \AA}$  for the latter work).

Let us now focus on the characteristics of the  $e(c)$  type galaxy population in a deeper detail. As we have already stressed in Sect. 5.1, these galaxies constitute a major component in local clusters and their luminosity distribution is quite distinct with respect to the other emission-lines types: not only it peaks at brighter values but, most important, it contains a substantial population of brighter objects, which is instead completely absent from the other two emission lines classes. If we look at the properties of the most luminous (i.e.  $M_V \leq -20$ ) tail of  $e(c)$  galaxies, and we compare them to the less luminous ones we note that:

- they have fainter [OII]: in most of them the equivalent width of this line is  $\geq -5 \text{ \AA}$ ;
- they have older ages (both mass- and luminosity-weighted: values are taken from Fritz et al., 2011);
- their spectra have redder (B–V) colour (median value of 1.0 against 0.8);
- they are on average more massive (a median mass of  $\sim 4 \times 10^{10} M_\odot$ , compared to a mean value of  $\sim 10^{10} M_\odot$  for the others).

In order to check whether this particular subsample is biased by noisy measurements of the [OII] line which is, for these cases, faint, we visually inspected the spectra and came to the conclusion that in the vast majority of cases the detection is real and the measure is reliable.

It is worth stressing that the detection of the [OII] line, which is the main feature used for classifying  $e(c)$ , distinguishing them from  $k$ , is not univocally related to the presence of a star forming activity in galaxies, but can instead have a different origin (see, e.g. Yan et al., 2006). Indeed, when inspected one-by-one, most of the high-mass ( $M_\star > 10^{10.5} M_\odot$ ) elliptical and S0 galaxies with an  $e(c)$  classification, display spectral features typical of LINERS or low-activity AGNs, such as an enhanced [NII] ( $6584 \text{ \AA}$ ) emission compared to  $H\alpha$ . This goes along the line of the findings by Yan et al. (2006), who pointed out that “[OII]-only” galaxies, or even those with a high [OII]/ $H\alpha$  ratio, are

more common among the reddest in their SDSS emission-lines sample, so probably the most massive ones. They classified as “post-starburst”, galaxies displaying a high [OII]/ $H\alpha$  ratio (or even with a [OII] detection, but no  $H\alpha$ , the so-called [OII]-only galaxies), and these were found to have red colour, similar to those in our subsample.

In fact, while we find ellipticals to represent only about 10% of  $e(a)$  and  $e(b)$  galaxies, the occurrence of this morphological type among the  $e(c)$  is higher than 20%, and it is mainly populated by the most luminous ones.

The occurrence of the [OII] line as well as other emission lines in local elliptical galaxies, is an already known phenomenon (see e.g. Caldwell, 1984; Phillips et al., 1986). These are either passive galaxies that are showing a residual, very low star formation level, or LINERS. A number of mechanisms other than star formation can be responsible for the production of the ionizing flux needed for the formation of forbidden lines: the presence of blue and evolved stellar populations, such as Horizontal Branch (HB) or post-asymptotic giant branch (post-AGB) stars, energetic gas shock waves or cooling flows. Post-AGB stars in particular seem to be one of the most likely sources for such spectral features, as a recent work by Singh et al. (2013) demonstrates, especially for massive galaxies, with very low level of star formation activity as those in our bright  $e(c)$  sample.

This issue is, of course, much easier to deal with for us as far as type-1 AGNs are concerned, as they are easily recognized by our spectral fitting routine. Given their extremely blue continuum and the presence of very broad emission lines, which are not compatible with the typical spectral features of stars, in such cases it is not possible to obtain an acceptable fit by means of SSP spectra. Like this, a high  $\chi^2$  value is returned, so that it is possible to easily recognize these objects with a targeted visual inspection.

Type-2 AGNs and LINERS have instead been identified in our spectra by fitting the underlying stellar continuum and investigating lines ratio diagnostic diagrams, as will be described in detail in Marziani et al. (in prep.). However, only 0.8% of the galaxies in our cluster sample turn out to

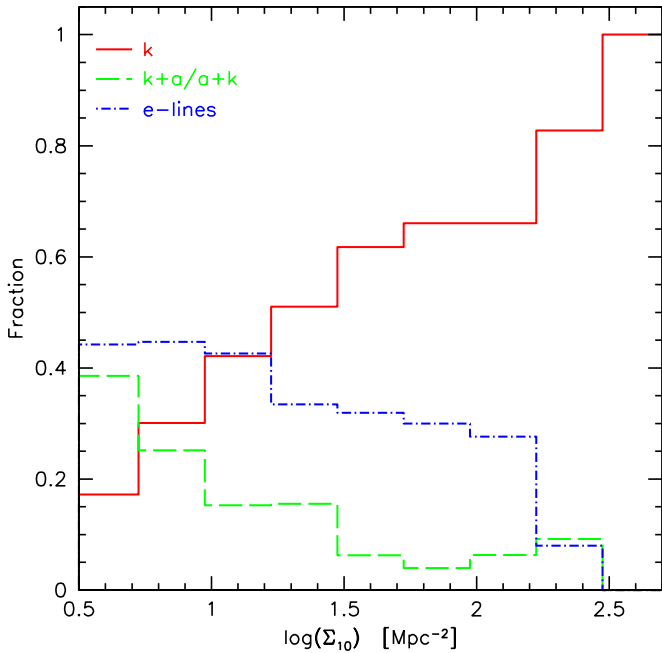


**Fig. 8.** Percentage of the passive, post-starburst and emission-lines types as a function of the (projected) local density.

be AGNs (either Seyfert-1 or Seyfert-2), therefore they are a negligible component of our spectroscopic sample.

In view of these considerations, we argue that part of the  $e(c)$ -classified objects, might very likely be constituted by galaxies with characteristics very similar to the passive class  $k$  (see Sect. 5.6), but hosting either some very low-energy LINER activity, or being influenced by one or more gas ionizing mechanisms as outlined above.

The location of a galaxy with respect to its companions and neighbours in a cluster, the so-called local density, plays an important role in shaping and defining some of its characteristics. The values of the projected local density that we will use are calculated from a circular area enclosing the first 10 most nearby galaxies, also accounting for background counts as expected from Berta et al. (2006), and corrected for border effect (see Vulcani et al., 2012, for details). The local density is expressed as the logarithm of the number of galaxies with  $M_V \leq -19.5$  per  $\text{Mpc}^{-2}$ .

In Fig. 8 we show the fraction of galaxies of the different spectral types, grouped into the three broad classes of passive ( $k$ ), emission-lines [ $e(a)$ ,  $e(b)$  and  $e(c)$ ] and post-starburst ( $k+a$  and  $a+k$ ), at different values of the local density, displayed in bins of 0.25 dex. Emission-line galaxies dominate the regions at the lowest densities, but their relative number monotonically decreases as the local density increases, and they are basically not found at the highest values.

Keeping the three emission-line classes separate slightly increases the noise in this plot, and the interpretation does not significantly change.  $e(a)$  and  $e(b)$  share a similar distribution with respect to the local density, and they are both extremely rare at densities above  $\sim 60 \text{ Mpc}^{-2}$  ( $\log[1.75]$ ): no more than 13% of galaxies in these two classes are found beyond those densities. A very similar trend is found for  $e(c)$ 's, whose distribution extends, instead, towards slightly

higher density values, being the main responsible for the tail at high values observed in Fig. 8. The three emission-line classes are distributed in a very similar manner compared to the two post-starburst classes, all of them displaying a peak between  $\log(1.25)$  and  $\log(1.50) \text{ Mpc}^{-2}$  in their distribution.

### 5.5. The properties of the Post-Starburst population

The  $k+a$  and  $a+k$  spectral classes, often referred to as post-starburst or post-star forming, make up about the 11% of the local cluster population at magnitudes brighter than  $-18$  ( $\sim 10\%$  and  $\sim 1\%$  for the  $k+a$  and  $a+k$ , respectively). This number is in strong contrast with the value found from the catalog of local cluster of Dressler & Shectman (1988), but broadly consistent with a fraction of  $\sim 15\%$  found among lower luminosity galaxies in 5 low- $z$  cluster by Caldwell & Rose (1997). The reason for the striking difference with the sample of Dressler & Shectman (1988) is probably due to the difference in the magnitude limit of the two surveys.

As described in Sect. 5.3, when viewed as two separate classes,  $k+a$  galaxies tend to have morphological characteristics very similar to passive objects, with a slight preference towards later morphological types, while  $a+k$  are more similar to the emission line types in this respect. This would fit the picture in which  $a+k$  galaxies are the direct descendants of emission line objects, especially star-bursting such as the  $e(b)$  types, gradually arising some  $10^7$  years after the star formation has stopped, when the most massive stars, providing the UV radiation necessary for the production of lines in emission, have already died. Furthermore, the fact that no  $k+a$  and  $a+k$  are classified as Sd/Irregular, argues against merging as the main mechanism to produce such spectra, and is in the line of the findings of Dressler et al. (1999) in clusters at high- $z$ : other processes must be the main responsible for the presence of such galaxies in clusters. Ma et al. (2008) reached a similar conclusion by studying a massive cluster at  $z=0.55$ , being able, by analysing the positions and velocities they display in the cluster, to rule out mergers as the dominant mechanism driving their creation and evolution, at least in clusters.

Remarkably enough, while not extremely different in the distribution of the morphological types,  $k+a$  and  $k$  galaxy differ substantially both with respect to their mass and luminosity function (see also Sect. 5.6); this is expected as an effect of downsizing, where the most massive galaxies have already evolved into passive types.

We note that there is a significant difference in the V-band luminosity distribution between the two post-starburst classes (see Fig. 5), with the  $k+a$  displaying a tail towards high luminosity, which is completely missing in  $a+k$ . This might be an indication that, at least part of the  $k+a$  types (the high luminosity ones), are not coming from  $a+k$ .

As the number of  $a+k$  is quite small when compared to all the other classes, in the rest of our analysis we will consider these two classes as one, adopting the broad definition of post-starburst for both.

Similarly to what we find for emission line galaxies, we do not see any correlation between the fraction of post-starburst and the cluster velocity dispersion or X-ray luminosity (see Fig. 9): the average fraction, calculated over all the clusters, is  $8.7 \pm 5.4$ . This is at odds with results

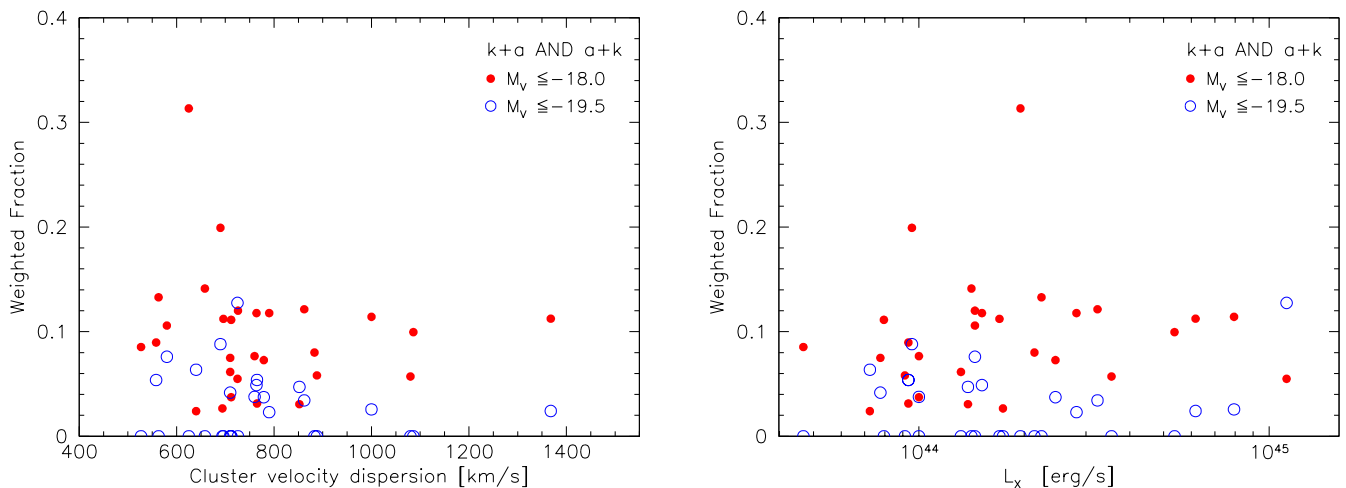


**Fig. 9.** Fraction of post-starburst galaxies, again as a function of the two cluster mass tracers, velocity dispersion (*left*) and  $L_X$  (*right*).  $k+a$  and  $a+k$  are considered as one single class. As done for Fig. 7, only galaxies within  $R_{500}$  are taken into account. Points with different colours refer to different magnitude limits and will be used later on for a comparison with high redshifts samples.

in the distant clusters, where the incidence of such galaxies strongly correlates with the cluster velocity dispersion (Poggianti et al., 2009b).

Poggianti et al. (2009b) define as “quenching efficiency” the ratio between the number of post-starburst and the active fraction, where “active” includes both emission line galaxies, but also the recently star forming classes  $k+a$  and  $a+k$ . We check whether this fraction, computed from weighted counts, correlates with any of the cluster properties. The value we have calculated by averaging over each cluster in our sample is  $20.7 \pm 11.7\%$ , and we see no significant dependency on either the X-ray luminosity or the velocity dispersion.

The post-starburst class has, in general, properties which are in between the passive and the star-forming galaxies. For example, the stellar mass distribution peaks at mass values which are intermediate between the  $k$  and the  $e(a)$  and  $e(b)$  class (see Fig. 6). The projected radial distribution of the spectral types tells a similar story: passive galaxies display the average tendency of gathering towards the cluster centre, while emission lines objects are more frequent in the outskirts, and post-starbursts occupy a region somehow in between. This can be clearly seen in the left-hand panel of Fig. 10, where we plot the cumulative radial distribution of WINGS spectral type, broadly divided in 3 classes.

On the right-hand panel of the same figure, we show the average velocity dispersion in 4 bins of projected radial distances. The average velocity dispersions of the post-starburst class have generally intermediate values between the passive and emission line classes, as if they were in an intermediate state of virialization between the passive and actively star-forming galaxies. The result we get by combining the information provided by the two panels in this Figure, indicates ram-pressure stripping as the most effective mechanism for the creation of a  $k+a/a+k$  spectrum. When a galaxy falls into a cluster, star formation is triggered as it reaches the cluster’s virial radius (e.g. Byrd & Valtonen, 1990; Fujita, 1998), and it is then abruptly

quenched once the galaxy enters deeper into the cluster environment and its interstellar medium gets very efficiently stripped by the intracluster hot gas (Gunn & Gott, 1972; Treu et al., 2003; Ma et al., 2008; Abadi et al., 1999). The fact that we see post-starburst galaxies in a shell-like radial distribution, somehow suggesting they define a transition region, might indeed be reflect the result of such a picture.

Finally, when considering the influence of the environs onto a galaxy through the local density (see Fig 8), post-starbursts quite follow the trend of emission lines galaxies, contributing gradually less to the total population, as the local density increases. Already at densities values larger than  $\sim 30 \text{ Mpc}^{-2}$  they make up only the 10% of the total galactic population, while being almost as numerous as the emission line class at the lowest density values.

### 5.6. Passive galaxies

This class includes all those galaxies whose spectrum does not show any [OII] emission (see Sect. 4.1 and Tab. 3) and weak  $H\delta$  absorption. By adopting this definition, we can consistently compare the properties of galaxies in our sample to those at higher redshift. Of course, this potentially leaves out other lines such as, for example, the  $H\alpha+[NII]$ , triplet which could in principle be detected even when no [OII] emission is measured. We checked the values of the  $H\alpha$  line in the  $k$  sample, and found that in only  $\sim 2\%$  (57 spectra) our method was able to detect an emission. These 57 objects do not show any preference in the values of the stellar mass or luminosity or other specific common properties.

As already shown, the great majority of  $k$  galaxies are early types, from a morphological perspective, around the 86% of them being classified as either ellipticals or S0s. This class is also dominated by higher luminosity galaxies, and the luminosity distribution, peaking at  $M_V \simeq -20.5$ , is radically different from that of any of the other classes.

Similarly, the stellar mass distribution is substantially different from that of the other 5 spectral classes: this class

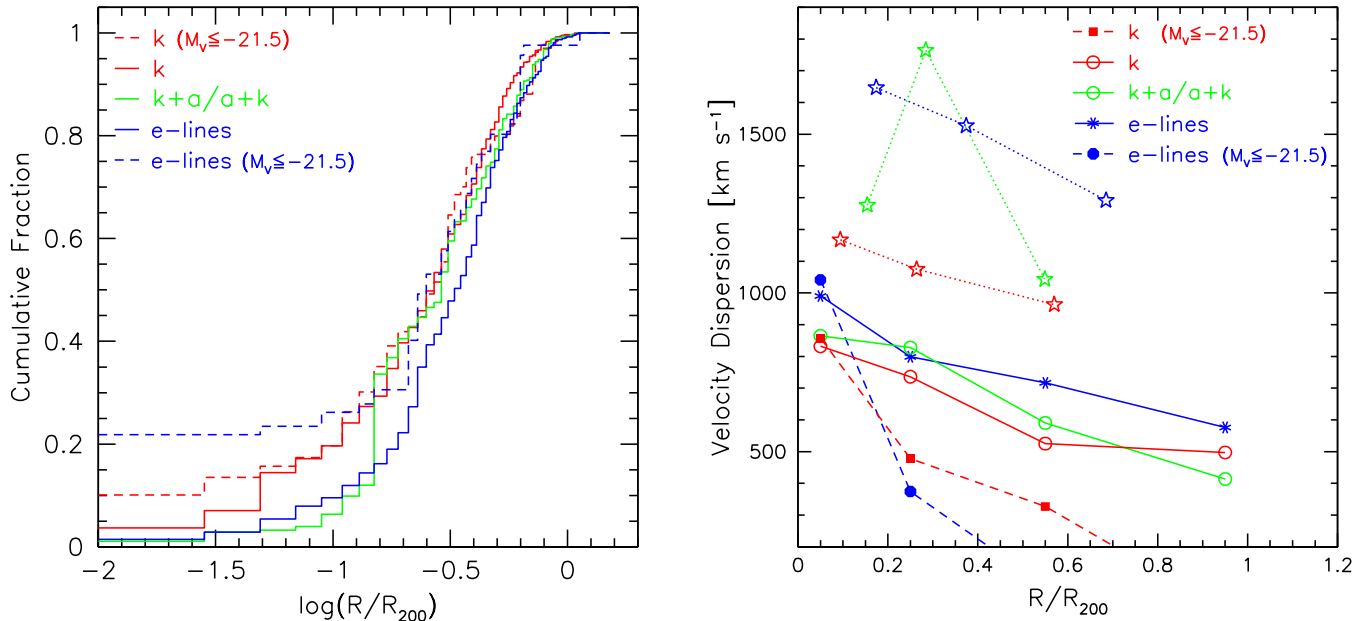


**Fig. 10.** On the *left-hand* panel: cumulative radial distribution of the three spectral types as defined in the text. On the *right-hand* the average velocity dispersion in bins of radial distance, for the three main spectral classes. Void stars represent the high- $z$  data points from Dressler et al. (1999). In all cases the distances are calculated from the cluster’s BCG, and are expressed in terms of  $R_{200}$ .

hosts the most massive galaxies, and only 20% of them have a mass lower than  $10^{10} M_{\odot}$  in our magnitude limited sample, in clear contrast with all the other classes where most of the galaxies have instead masses below that limit (see Fig. 6); the  $e(c)$  galaxies are the only exception.

Following what done for the  $e(c)$  type, we distinguish passive galaxies in two ranges of V-band luminosity as well, namely brighter and fainter than  $M_V = -21.5$ . As noted by Biviano et al. (2002) (but see also Beisbart & Kerscher, 2000), the brightest early types should display the highest degree of segregation.

This is somehow confirmed for the WINGS sample as well, as it can be seen in the left-hand panel of Fig. 10: the high-luminosity  $k$  spectral type galaxies are proportionally more numerous than all other spectral types (with the exception of the luminous emission-lines, which we have already discussed in Sect. 5.4), in the very central regions of clusters, even though the difference is not as evident as the one found by Thomas & Katgert (2006).

As for the distribution of the passive class as a function of the local density, Fig. 8 clearly shows how galaxies in this class are the ones detected in the widest range of projected densities, with objects found in basically any kind of local environment. They make up about the 60% of the galaxies at densities larger than  $\sim 50 \text{ Mpc}^{-2}$ , and they are basically the only ones found, in our magnitude-limited sample, at  $\Sigma_{10} \gtrsim 100 \text{ Mpc}^{-2}$ .

### 5.7. Galaxies in local clusters

In this section we give a summary of the properties which describe the local population of cluster galaxies, and the picture which emerges from our analysis. This allows to

more easily compare low and high- $z$  galaxies, as we do in the following Section.

About 50% of the galaxies in local clusters have spectra resembling those of passively evolving objects, while almost 40% display emission lines and only about 10% show the signatures typical of objects in a post-starburst/post-starforming phase (see Table 3). Passive galaxies are not only, on average, the most massive ones, but also the most luminous, while the emission line classes clearly show a deficit of luminous/massive objects (see the left panel of Fig. 5). This picture very well fits the downsizing scenario, in which the most massive galaxies are the first that are formed, and are already evolving in a passive fashion (i.e. following the stellar evolution) since at least  $z \sim 1$  (e.g. De Propris et al., 2007; Andreon, 2008; Strazzullo et al., 2010), while at progressively lower masses we find objects with increasingly higher specific star formation rates.

A remarkable exception to this picture is that of the  $e(c)$  class, which contains a family of luminous (and more massive than the average) galaxies almost resembling the high luminosity tail of the passive type. When analysed with a closer look, these turn out to have characteristics which are very similar to those of the  $k$ ’s, being only different in the presence of the [OII] line which is anyway —on average— not very intense and it is likely produced by physical processes different than star formation.

When comparing the luminosity functions of the spectral types, it is tempting to view them as mirroring an evolutionary sequence, going from the star-forming  $e(b)$  and  $e(a)$ , containing the least luminous galaxies, to the more “extreme” post starburst class  $a+k$ , whose luminosity distribution is similar to that of the  $e(b)$  and  $e(a)$ ’s; containing a higher fraction of luminous object, galaxies in the  $k+a$  class are characterized by a luminosity distribu-

tion in between the star-forming and the passive types  $k$  which host, in turn, the most luminous objects. The  $e(c)$  are, once again, an exception to this scheme, both because their classification might be influenced by the nature of the [OII] line production, and because they probably contain the field galaxies which are being accreted by the clusters and will eventually end up “feeding” the high luminosity tail of the  $k+a$  family.

Contrary to the findings of Poggianti et al. (2009a), who found the spirals fraction in WINGS clusters to correlate with the X-ray luminosity, we note how neither the fraction of emission-lines galaxies nor that of post-starbursts, depends on the global properties of the cluster, specifically on the clusters’ velocity dispersion or their X-ray luminosity, as it can be noted from Fig. 7 and Fig. 9. What drives the spectral characteristics is instead the local environment, as the dependence of the spectral type on the projected local density demonstrates (see Fig 8): galaxies in dense environment tend to have their star formation quenched.

## 6. A comparison with the high-redshift clusters population

In this section we attempt a comparison of some of the properties of the local cluster galaxies with those at higher redshift. This way, we can trace the evolution of these properties as a function of the cosmic time, to shed some light on the physical mechanisms that drive of the physical and structural changes of galaxies in dense environments.

Two surveys provide samples which turn ideal to perform such a comparison: one was collected by the MORPHS<sup>1</sup> collaboration, which observed galaxies in clusters at redshifts in the 0.37 – 0.56 range; the second is the ESO Distant Cluster Survey<sup>2</sup> (EDisCS; White et al., 2005), targeting instead cluster galaxies with redshifts between 0.4 and  $\sim 1$ .

To properly compare the high- $z$  samples and WINGS, minimizing the effect of possible biases, the magnitude limits of these surveys must be matched and, furthermore, these must be also corrected to account for evolution effects. That is, the changes occurring in the mass-to-light ratios as the stellar populations in galaxies gets progressively older at different cosmic ages, should be taken into account. If we assume that stellar evolution is the only mechanism acting in the luminosity change, and if we consider a common redshift of formation, we can exploit stellar populations models to calculate the change in luminosity from redshift 0.55 to redshift 0.04 which represent the most extreme difference between WINGS and MORPHS. Assuming that the oldest stars are as old as the Universe at a given redshift, we compare the V band luminosity of simple stellar populations with an age as close as possible to the age of the Universe at  $z = 0.04$  and  $z = 0.55$ , that is  $T_U \simeq 12.9$  and  $T_U \simeq 8.08$  Gyr, respectively. The difference is, assuming a solar metallicity and a Salpeter (1955) IMF, of  $\sim 0.3$  magnitudes.

In their analysis of EDisCS galaxies, Poggianti et al. (2009b) use a cut in absolute V-band magnitude at  $M_V = -20.1$  at  $z = 0.4$ , which corresponds to  $M_V = -19.8$  for WINGS, while in the work by Dressler et al. (1999) using MORPHS data, the completeness limit is  $M_V = -19 + 5 \cdot \log_{10} h$ , corresponding to about  $M_V = -19.5$  for WINGS.

We will use this latter value to compare the high and low redshift galaxies, but we have verified that using -19.8 does not change our results.

### 6.1. Occurrence of the spectral classes

We find that post-starburst galaxies in local clusters are less abundant with respect to their analogous at high redshift. To our  $M_V < -18$  magnitude limit we have classified about the 11% of the local cluster population as post-starburst (i.e. either a  $k+a$  or a  $a+k$ ). At brighter magnitudes, matching the limits of the two aforementioned high redshift studies, the post-starburst fraction is 18% at high- $z$  (as calculated for MORPHS galaxies by Dressler et al., 1999), while it lowers down to 4.6 % in the WINGS clusters (if we assume a brighter limit, at  $M_V < -19.8$  the fraction further reduces to 4.4%). These numbers are spot on those predicted by Poggianti et al. (2009b) for  $z \simeq 0$  clusters, under the hypothesis that the star formation quenching efficiency is similar between local and distant clusters. In fact, assuming post-starburst galaxies are formed after star formation is stopped in infalling star forming systems, and adopting the same value of the quenching efficiency –as defined in Sect. 5.5– of 23%, calculated at high redshift, and a star forming fraction of 20% for the local clusters (taken from the study of Poggianti et al., 2006, exploiting SDSS data), the expected fraction of local post-starburst would be 4.6%.

Indeed, if we calculate the quenching efficiency for galaxies in the WINGS sample, we find a value of  $22.0 \pm 0.6\%$ , which reduces to  $15.5 \pm 1.0$  if a magnitude limit of -19.5 is considered. In their work, using both EDisCS and MORPHS data, Poggianti et al. (2009b) found a dependency of the quenching efficiency to the cluster velocity dispersion (see their Fig.5), which is particularly evident for the highest velocity dispersion values. This dependence is instead absent in WINGS clusters (see discussion below). Hence, the aforementioned  $\sim 15\%$  value is mainly to be intended for clusters with velocity dispersions below  $\sim 1000$  km/s and is, within this limit, in fairly good agreement with the high- $z$  result.

Unlike their higher redshift progenitor, we find at most a weak dependence of the relative incidence of post-starburst galaxies on total cluster mass as traced by the velocity dispersion and the X-ray luminosity. Looking at Fig. 9 it is especially evident that there is a flat trend in the occurrence of these class as a function of the cluster X-ray luminosity, while it seems instead that a weak anticorrelation is present when the same quantity is considered as a function of the velocity dispersion. This is compatible with the interpretation that the cluster mass at low- $z$  has little or no effect in producing this particular spectral class, in particular at low luminosities where we find most of them.

At the high redshift magnitude limit, the WINGS sample is dominated by the passive  $k$  type, containing 2/3 of the whole population, a significantly higher fraction with respect to the 47% found in Dressler et al. (1999). Meaningful differences are also found for the emission line galaxies: the fraction of  $e(a)$  reduces from 11% to a local value of 2% and, at these bright absolute magnitudes, the  $e(b)$  class almost disappears declining from a 16% to less than 1%, clearly revealing the well known Butcher-Oemler effect. Instead, the continuous star-forming like spectrum  $e(c)$  experiences an increase when going from high to low redshifts, moving from

<sup>1</sup> <http://www.astro.dur.ac.uk/~irs/morphs.html>

<sup>2</sup> <http://www.mpa-garching.mpg.de/galform/ediscs/>

a bare 5% to 27%, locally. While part of this increase might come from high- $z$   $e(b)$  galaxies progressively slowing down their star forming activity, this is barely enough to make up the local  $e(c)$  fraction. Two effects might explain this high number of local luminous  $e(c)$  we measure, in comparison to high redshift clusters. The first is of methodological nature, and might arise from the lower detection limit that we have assumed for the [OII] lines –  $EW = -2 \text{ \AA}$  vs  $-5$  –, which discriminates between the  $e(c)$  and  $k$  type. If this was the reason, we would end up having a even larger fraction of local  $k$  galaxies. Indeed, if we assign a  $k$  classification to ALL those  $e(c)$  galaxies with  $EW([OII]) > -5 \text{ \AA}$ , their fraction would considerably reduce, moving to a much lower 14%, while passive  $k$ -type galaxies would become the dominant galaxies containing almost 80% of the objects. Still, this is far from the 5% fraction observed at high- $z$ .

In fact, we could be observing a second, more phenomenological effect, as the different  $e(c)$  fraction might reflect the way star formation proceeds in field galaxies that have been recently captured by the cluster, at a lower and steadier pace at lower redshift as opposed to a higher and bursty-like activity at high redshift.

Finally, we note a drastic decrease in the incidence of  $e(a)$  galaxies (from 11% to 2%) as well. These are unlikely to have turned into the  $k+a$  or  $a+k$  we observe in WINGS clusters, as long as passive evolution only is considered (i.e. no merger or gas accretion events). In fact, the time scale during which the spectral features typical of A-stars dominate is around  $\sim 1$  Gyr, much shorter than the 5 Gyr period separating the redshift range we are investigating, and after which the Balmer lines become progressively fainter and, if star formation has ceased, such galaxies would eventually end up showing a  $k$  spectrum.

Another quite striking aspect differentiating WINGS and MORPHS galaxies concerns the morphological properties. Generally speaking, when compared to the high- $z$  sample, we note the absence of irregular galaxies among the local  $k$ ,  $k+a$  and  $a+k$  spectral type, and a much lower incidence of the later morphological classes. In fact, in the distant sample, most post-starbursts are classified as late-type, with only  $\sim 27\%$  of the objects being assigned an ellipticals or S0 morphology (but see also Tran et al., 2003, for a similar results on a study at comparable redshift). This number compares to a much higher fraction ( $\sim 70\%$ ) of low redshift galaxies which have instead a morphological early type (E or S0) classification.

## 6.2. The Luminosity distributions

Dressler et al. (1999) presented a comparison of the V-band luminosity functions for 6 spectral types, whose definition matches the one we have adopted for this work. In Fig. 11 we plot those same luminosity distributions, which we have corrected as explained above to account for passive luminosity evolution, together with the local ones. Having in mind that the high- $z$  sample is to be considered complete for  $M_V \lesssim -19.5$ , thus limiting the analysis to the brightest galaxies, we can consistently compare the two samples.

Galaxies with the strongest emission lines –  $e(b)$  – are lacking a significant presence of objects more luminous than  $M_V < -20$  throughout all the redshift range here considered. From the uppermost panel of Fig. 11, it is tempting to claim that higher redshift star bursting galaxies are in general more luminous compared to their most nearby

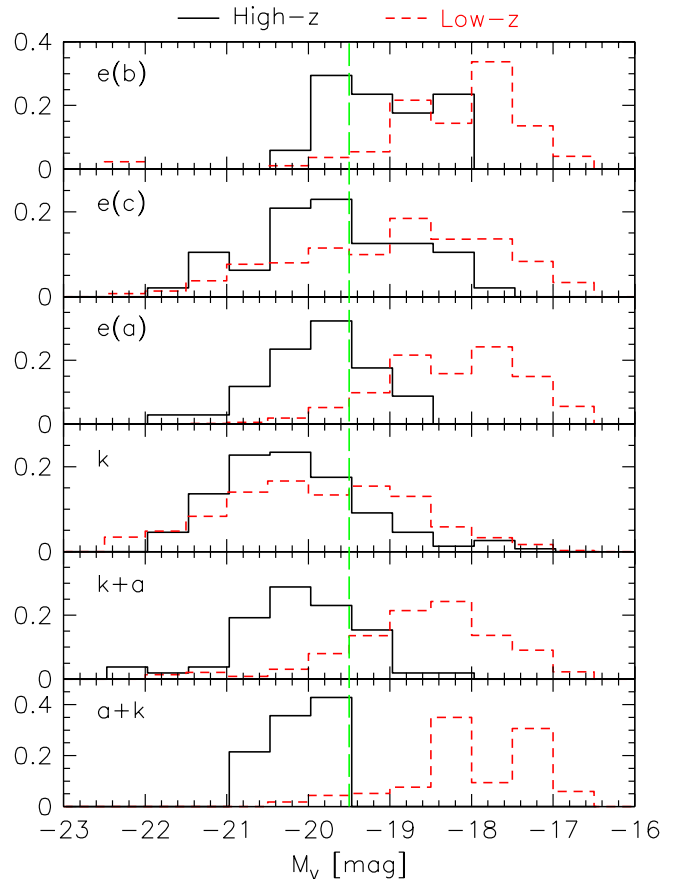


**Fig. 11.** Comparison of the high and low redshift V-band luminosity distribution for the 6 spectral types. High- $z$  data have been corrected for passive evolution so to match the local clusters data (see text for details). The vertical dashed line marks the  $M_V = -19.5$  limit.

counterparts, even though incompleteness at high redshift might be driving, at least partially, this comparison. Very luminous star bursting galaxies are anyway not observed in local clusters, but nothing more can be said on their luminosity distribution based on these datasets.

Taking magnitude limits into account, the luminosity of  $e(c)$  galaxies turns out to be very similar at these redshifts, while the  $e(a)$  types mostly differ due to the presence of a significantly brighter population in the MORPHS sample, which is compatible with the luminosity distribution of the low-redshift  $k+a$  class. It seems anyway unlikely that the high redshift  $e(a)$  can be considered as the progenitors of the local  $k+a$ , as the elapsed time since  $z \sim 0.5$  to now is a factor of 3-4 higher than the life of the A stars features, unless they host a significant amount of obscured and prolonged star formation which will eventually leave its  $k+a/a+k$  signature in local clusters.

The luminosity functions of  $k$  galaxies at low and high redshift are quite similar. Interestingly, above  $M_V = -22$ , the local population contains a slightly higher number of brighter objects. This could either be due to a somehow incomplete sampling of the high-redshift population (the MORPHS sample only contains 10 clusters, as opposed to the  $\sim 30$  in WINGS), or it could be a real evolution effect, for which these passive galaxies would have under-

gone dry-merger events, having left their spectral features unchanged, while only increasing their luminosity.

A significant difference can also be observed in the post-starburst class galaxies, whose high- $z$  sample displays a) a slightly more luminous tail, b) a higher number of galaxies with higher luminosities, and c) a significantly different peak magnitude,  $\sim -20.2$  vs  $\sim -18.5$  (even though the latter value may be limited by incompleteness) at high and low  $z$ , respectively. Once again, this fits a downsizing galaxy evolution scenario, in which the most active galaxies are those at progressively lower mass (luminosity) as one moves from high to the low redshift Universe.

### 6.3. Spectral properties and the position in the cluster

Finally, we compare the radial distribution of the spectral types for the different surveys. We consider only 3 main spectroscopic classes: emission line galaxies, passive galaxies, including only the spectroscopic type  $k$  and the  $k+a$  and  $a+k$ .

In the left-hand panel of Fig. 10, we plot the cumulative radial distribution of the three spectral types defined above. At low redshift, the  $k$  type galaxies, and in particular the brightest ones ( $M_V \leq -21.5$ ), are the most centrally concentrated, while emission-line galaxies tend to prefer the clusters' outskirts, and the post-starburst population generally sits at an intermediate region between the two. 50% of  $k$  galaxies are found within a projected radial distance of  $\sim 0.25 \cdot R_{200}$ , while the same percentage for the emission line ones is reached at  $\sim 0.40 \cdot R_{200}$ , showing the tendency to avoid the innermost regions of the clusters, which are dominated by the early-type, passive population.

Although this analysis inevitably suffers from projection effects, it still provides some clue to how the characteristics of the galaxies are, on average, shaped by the environment. These trends are similar to those found in distant clusters by both Dressler et al. (1999) and Poggianti et al. (2009a), even though the differences between the three aforementioned classes seem to be less evident for our sample. If, at low redshift, we limit our comparison to the sample matching the distant clusters absolute magnitude, the situation does not change for emission line and passive galaxies, even though the radial distribution for post-starbursts becomes noise-dominated, being hampered by the very low number of objects at this magnitude limit.

We compare also the radial distribution of the velocity dispersions for the spectral classes, which we have shown in the right panel of Fig. 10 for WINGS galaxies, between the high (MORPHS) and low  $z$  clusters. In general, we find that the values measured in WINGS clusters are up to  $\sim 50\%$  lower with respect to the higher redshift counterparts, most likely due to the achievement of a more advanced state of virialization of the local clusters. Apart from this, the average trend which sees the early types having the lowest velocity dispersion at any radius, and the late types displaying a similar trend but at higher velocities, is also seen in local clusters, even though at a much higher dispersion. Furthermore, the decline of the velocity as a function of the projected radius, is quite similar for the two samples, in all the spectral classes.

What is significantly different in local clusters is the average difference, in velocities, in particular between passive and emission-lines galaxies, which are instead clearly distinct at high- $z$ . Overall, the velocity dispersions between the

different spectral types at low redshift is much more similar, with an average ratio  $\sigma_e/\sigma_k = 1.22 \pm 0.11$ , only marginally consistent with the  $1.40 \pm 0.16$  ratio of the MORPHS sample.

## 7. Summary and conclusions

In this paper we have presented a catalog of equivalent widths of the most prominent spectral lines in the  $\sim 3700$  to  $6600 \text{ \AA}$  range, automatically measured in medium resolution spectra from the WINGS spectroscopic survey. We use these measures to classify galaxies based on the intensity and presence/absence of the  $H\delta$  and  $[OII]$  lines, and we focus our analysis on those objects which are spectroscopically confirmed cluster members. This classification reflects the stellar content of a galaxy, and is widely used as a mean to derive clues on the star formation history both locally and at higher redshifts.

Together with other physical parameters and characteristics of the WINGS galaxies sample derived in previous works such as morphology (Fasano et al., 2012), stellar mass and absolute magnitude (Fritz et al., 2011), we investigate the properties of the different spectral types, trying to understand how the characteristics of the stellar populations vary as a function of other galactic properties and of both local and global environment, in local clusters.

Having used a classification scheme which is adopted by several other studies at higher redshifts, we can then compare the characteristics of local cluster galaxies to their more distant progenitors.

We can summarize our results as follows:

1. the local cluster population at magnitudes  $M_V \leq -18$  is dominated by the passive  $k$  spectral type, followed by  $e(c)$  galaxies, even though possibly contaminated – especially at high luminosity (or stellar mass) – by emission line from non-stellar origin. About 11% of galaxies display a post-starburst spectrum;
2.  $k$  galaxies are not only the most luminous ones, but they also display the broader range of V-band luminosities. The  $e(c)$ 's have a similar spread, but a significantly lower ( $\sim 1.5$  magnitudes) peak luminosity;
3.  $k$  galaxies are also the slowest in clusters (see Fig. 10, right-hand panel). This is consistent with early types being on average more virialized with respect to late types, and with the findings that they were already in place since  $z \simeq 0.6$  (see, e.g. Smail et al., 1997);
4. there is a broad correlation between the morphological and the spectroscopical classification: more than 80% of the  $k$  and  $k+a$  spectra are ellipticals or S0s, while the majority of the recently star-forming galaxies [ $e(a)$ ,  $e(b)$  and  $a+k$ ] are spirals. The  $e(c)$  class is almost equally populated by early (E+S0) and late (Sp) morphological types. Yet, the fact that most of the spectral types display a full range of morphologies, suggests that the evolution of these two properties is, at least partially, decoupled;
5. no significant correlation is found between the relative number of emission-line galaxies and the cluster general properties, such as their X-ray luminosities or velocity dispersion;
6. the local density, instead, clearly plays a role in the spectral type segregation: a great fraction of passive galaxies is found at the largest values of projected density, while

other spectral types are instead more common in less dense environment;

7. there is a fraction of the  $e(c)$  population showing substantial differences with respect to the other emission line classes: they display properties more similar to the passive type. We argue that, in this particular case, part of them might be  $k$  type galaxies where the [OII] line is not related to star formation, but has instead a different origin;
8. we confirm the lack of local high luminosity post-starbursts, strengthening the idea that these galaxies have undergone a significant evolution. The luminosity function is also significantly different with respect to the one at high redshift;
9. local post-starbursts display the tendency to prefer earlier morphological types, compared to the high redshift ones (i.e. no irregular  $k+a$  and  $a+k$  are found in the WINGS sample);
10. the star formation quenching efficiency is similar between high and low redshift, as long as clusters with velocity dispersions less than  $\sim 1000$  km/s are considered, with some differences possibly due to downsizing effects. This strongly suggests RAM-pressure stripping as the main mechanism for halting star formation in infalling galaxies, across the  $z \sim 0 - 1$  redshift range.

Finally, we briefly describe the EW catalog (see an example of the typical quantities and format in Appendix A), which is made publicly available through both the CDS and the Virtual Observatory. More details on this catalog and, in general, on WINGS and its products can be found in Moretti et al. (subm.).

## ACKNOWLEDGMENTS

This work made use of Virtual Observatory tools, namely TOPCAT (<http://www.star.bris.ac.uk/~mbt/topcat/>).

Facilities: Anglo Australian Telescope (3.9 m- AAT); William Herschel Telescope (4.2 m- WHT).

Funding for the SDSS and SDSS-II has been provided by the Alfred P. Sloan Foundation, the Participating Institutions, the National Science Foundation, the U.S. Department of Energy, the National Aeronautics and Space Administration, the Japanese Monbukagakusho, the Max Planck Society, and the Higher Education Funding Council for England. The SDSS Web Site is <http://www.sdss.org/>.

We are grateful to the anonymous referee, whose comments and remarks helped us to improve the readability of this work.

## References

- Abadi, M. G., Moore, B., & Bower, R. G. 1999, MNRAS, 308, 947  
 Andreon, S. 2008, MNRAS, 386, 1045  
 Balogh, M. L., Morris, S. L., Yee, H. K. C., Carlberg, R. G., & Ellingson, E. 1999, ApJ, 527, 54  
 Beisbart, C., & Kerscher, M. 2000, ApJ, 545, 6  
 Bekki, K., Shioya, Y., & Couch, W. J. 2001, ApJ, 547, L17  
 Bell, E. F., & de Jong, R. S. 2001, ApJ, 550, 212  
 Berta, S., Rubele, S., Franceschini, A., et al. 2006, A&A, 451, 881  
 Biviano, A., Katgert, P., Mazure, A., et al. 1997, A&A, 321, 84  
 Biviano, A., Katgert, P., Thomas, T., & Adami, C. 2002, A&A, 387, 8  
 Bruzual A., G. 1983, ApJ, 273, 105  
 Buote, D. A., & Tsai, J. C. 1995, ApJ, 452, 522  
 Butcher, H., & Oemler, A., Jr. 1978a, ApJ, 219, 18  
 Butcher, H., & Oemler, A., Jr. 1978b, ApJ, 226, 559  
 Butcher, H., & Oemler, A., Jr. 1984, ApJ, 285, 426  
 Byrd, G., & Valtonen, M. 1990, ApJ, 350, 89  
 Caldwell, N. 1984, PASP, 96, 287  
 Caldwell, N., & Rose, J. A. 1997, AJ, 113, 492  
 Cava, A., et al. 2009, A&A, 495, 707  
 Couch, W. J., & Sharples, R. M. 1987, MNRAS, 229, 423  
 Couch, W. J., Ellis, R. S., Sharples, R. M., & Smail, I. 1994, ApJ, 430, 121  
 Couch, W. J., Balogh, M. L., Bower, R. G., et al. 2001, ApJ, 549, 820  
 Dale, D. A., Giovanelli, R., Haynes, M. P., Hardy, E., & Campusano, L. E. 2001, AJ, 121, 1886  
 De Propriis, R., Stanford, S. A., Eisenhardt, P. R., & Dickinson, M. 2003, ApJ, 598, 20  
 De Propriis, R., Colless, M., Peacock, J. A., et al. 2004, MNRAS, 351, 125  
 De Propriis, R., Stanford, S. A., Eisenhardt, P. R., Holden, B. P., & Rosati, P. 2007, AJ, 133, 2209  
 Dressler, A. 1980, ApJ, 236, 351  
 Dressler, A., & Gunn, J. E. 1983, ApJ, 270, 7  
 Dressler, A., & Shectman, S. A. 1988, AJ, 95, 284  
 Dressler, A., & Gunn, J. E. 1992, ApJS, 78, 1  
 Dressler, A., Oemler, A., Jr., Couch, W. J., et al. 1997, ApJ, 490, 57  
 Dressler, A., Smail, I., Poggianti, B. M., Butcher, H., Couch, W. J., Ellis, R. S., & Oemler, A. J. 1999, ApJS, 122, 51  
 Dressler, A., Oemler, A., Jr., Poggianti, B. M., et al. 2013, ApJ, 770, 62  
 Fasano, G., Poggianti, B. M., Couch, W. J., et al. 2000, ApJ, 542, 673  
 Fasano, G., et al. 2006, A&A, 445, 805  
 Fasano, G., Vanzella, E., Dressler, A., et al. 2012, MNRAS, 420, 926  
 Fritz, J., et al. 2007, A&A, 470, 137  
 Fritz, J., et al. 2011, A&A, 526, A45  
 Fujita, Y. 1998, ApJ, 509, 587  
 Gladders, M. D., Oemler, A., Dressler, A., et al. 2013, ApJ, 770, 64  
 Goto, T., Nichol, R. C., Okamura, S., et al. 2003, PASJ, 55, 771  
 Goto, T., Yagi, M., Tanaka, M., & Okamura, S. 2004, MNRAS, 348, 515  
 Gunn, J. E., & Gott, J. R., III 1972, ApJ, 176, 1  
 Haines, C. P., Smith, G. P., Egami, E., et al. 2009, ApJ, 704, 126  
 Hausman, M. A., & Ostriker, J. P. 1978, ApJ, 224, 320  
 Kang, W., & Lee, S.-G. 2012, arXiv:1207.2845  
 Lavery, R. J., Pierce, M. J., & McClure, R. D. 1992, AJ, 104, 2067  
 Leonardi, A. J., & Rose, J. A. 1996, AJ, 111, 182  
 Longhetti, M., & Saracco, P. 2009, MNRAS, 394, 774  
 Ma, C.-J., Ebeling, H., Donovan, D., & Barrett, E. 2008, ApJ, 684, 160  
 Margoniner, V. E., & de Carvalho, R. R. 2000, AJ, 119, 1562  
 Newberry, M. V., Boroson, T. A., & Kirshner, R. P. 1990, ApJ, 350, 585  
 Phillips, M. M., Jenkins, C. R., Dopita, M. A., Sadler, E. M., & Binette, L. 1986, AJ, 91, 1062  
 Poggianti, B. M., Smail, I., Dressler, A., Couch, W. J., Barger, A. J., Butcher, H., Ellis, R. S., & Oemler, A. J. 1999, ApJ, 518, 576  
 Poggianti, B. M., Bridges, T. J., Komiyama, Y., Yagi, M., Carter, D., Mobasher, B., Okamura, S., & Kashikawa, N. 2004, ApJ, 601, 197  
 Poggianti, B. M., et al. 2006, ApJ, 642, 188  
 Poggianti, B. M., et al. 2009a, ApJ, 697, L137  
 Poggianti, B. M., Aragón-Salamanca, A., Zaritsky, D., et al. 2009b, ApJ, 693, 112  
 Postman, M., Lubin, L. M., & Oke, J. B. 2001, AJ, 122, 1125  
 Prugniel, P., Golev, V., & Maubon, G. 1999, A&A, 346, L25  
 Quintero, A. D., Hogg, D. W., Blanton, M. R., et al. 2004, ApJ, 602, 190  
 Riffel, R., & Borges Vale, T. 2011, Ap&SS, 187  
 Salpeter, E. E. 1955, ApJ, 121, 161  
 Sánchez-Blázquez, P., Jablonka, P., Noll, S., et al. 2009, A&A, 499, 47  
 Singh, R., van de Ven, G., Jahnke, K., et al. 2013, A&A, 558, A43  
 Smail, I., Ellis, R. S., Dressler, A., et al. 1997, ApJ, 479, 70  
 Sousa, S. G., Santos, N. C., Israelian, G., Mayor, M., & Monteiro, M. J. P. F. G. 2007, A&A, 469, 783  
 Stetson, P. B., & Pancino, E. 2008, PASP, 120, 1332  
 Strazzullo, V., Rosati, P., Pannella, M., et al. 2010, A&A, 524, A17  
 Thomas, T., & Katgert, P. 2006, A&A, 446, 31  
 Tonnesen, S., Bryan, G. L., & van Gorkom, J. H. 2007, ApJ, 671, 1434

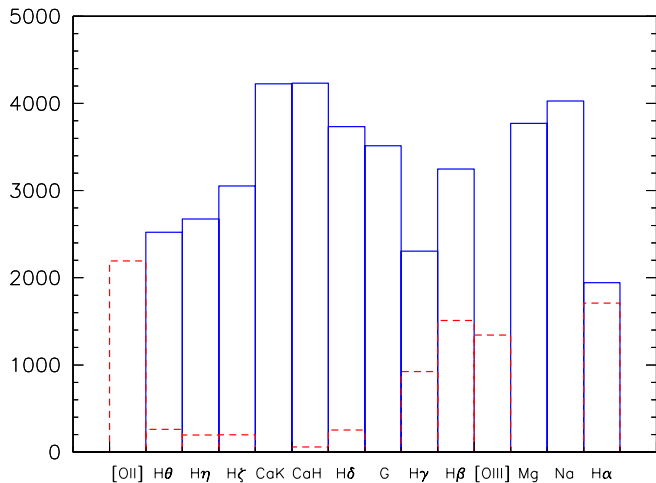


**Fig. A.1.** Statistics on the lines measurement. The histograms show the number of spectra for which a given line was properly measured. Red, dashed-line histograms refer to lines in emission ( $EW < 0$ ).

- Tran, K.-V. H., Franx, M., Illingworth, G., Kelson, D. D., & van Dokkum, P. 2003, *ApJ*, 599, 865  
 Treu, T., Ellis, R. S., Kneib, J.-P., et al. 2003, *ApJ*, 591, 53  
 Valentinuzzi, T., Woods, D., Fasano, G., et al. 2009, *A&A*, 501, 851  
 van Dokkum, P. G., & Franx, M. 2001, *ApJ*, 553, 90  
 Varela, J., et al. 2009, *A&A*, 497, 667  
 Vulcani, B., Poggianti, B. M., Fasano, G., et al. 2012, *MNRAS*, 420, 1481  
 White, S. D. M., Clowe, D. I., Simard, L., et al. 2005, *A&A*, 444, 365  
 Yan, R., Newman, J. A., Faber, S. M., Konidaris, N., Koo, D., & Davis, M. 2006, *ApJ*, 648, 281  
 Zabludoff, A. I., Zaritsky, D., Lin, H., et al. 1996, *ApJ*, 466, 104

## Appendix A: The Equivalent Widths catalog

The catalog presented in this paper contains EW values of 14 among the most prominent emission and absorption lines in the optical range (see Tab.1), measured in the rest-frame observed spectra. Errorbars on the measures, taking into account both the spectral S/N and the measurement method, are also provided, with the details of their calculation being explained in Sect.3.1. These values, those of the [OII] and H $\delta$  in particular, are used to derive a rough spectral classification, which is included in the catalog in the form of a numerical flag. Emission lines galaxies are labelled with 1,2 and 3 for  $e(a)$ ,  $e(b)$  and  $e(c)$ , respectively, while the “non-starforming” types are flagged with 4, 5 and 6 ( $k$ ,  $k+a$  and  $a+k$  respectively). Where no classification was possible we flag the spectrum with a 0. In Fig. A.1, we report the number of spectra in which each line was successfully measured, for the entire sample, and distinguishing those that were measured in emission (red histograms).

Non-detections and noise-dominated lines are flagged with a 99.00, while the value 999.00 is used to identify those lines that lie outside the observed range. We also measure two classical, widely used, indexes:  $D(4000)$  (Bruzual A., 1983) and  $D_n(4000)$  (Balogh et al., 1999). As already mentioned, whenever a [OII] and [OIII] EW have a value which is higher than  $-2 \text{ \AA}$ , a 0.000 value as a non-reliable detection, which is flagged by a 0.000 value. In the catalog we are also

reporting the values of the magnitude and radial completeness ( $C(m)$  and  $C(r)$ ). Table A.1 shows an example of how the catalogue looks like. Column 1 reports the WINGS name, based on the galaxy’s coordinate; columns 2 to 15 report the equivalent width values expressed in  $\text{\AA}$ ; columns 16 to 29 report the uncertainties, following the same order as the EW values; columns 30 and 31 contain the spectral indexes  $D4000$  and  $D_n4000$ , respectively; in column 32 we give the spectral class flag and in columns 33 and 34 we provide the photometric and geometrical completeness, respectively.

Note that – for the spectra of the north sample – since the measurements of lines shortwards of  $\sim 4300 \text{ \AA}$  is not reliable in most of them, for [OII], H $\delta$  and the two calcium lines (CaK and CaH+He) we give the values that were manually measured, while values for the other lines – longwards of  $4300 \text{ \AA}$  – are taken from the automatic measurement.

The presence of sky lines, which are not always properly subtracted from observed spectra, might also influence both the detection and the lines’ measurement. If we consider the most prominent of such lines, i.e. those at  $5577$ ,  $5894$ ,  $6300$  and  $7246 \text{ \AA}$ , we find that, as far as WINGS cluster members are concerned, only the Mg and the Na lines might fall close to these sky features, especially in the higher redshift clusters. None of the other lines are instead affected, but we strongly suggest a visual check before using the values for these two lines. Similarly, a visual check should be performed in the spectra of higher redshift, foreground galaxies in our samples. For example, spectra of galaxies at  $z \sim 0.108$ , will have both H $\alpha$  and the [OIII] lines critically close to such sky lines.

## Appendix B: Notes on the completeness

The parent catalog from which spectroscopic targets were selected has been generated adopting the following selection criteria:

1.  $V_{tot} < 20$
2.  $V_{fib} < 21.5$
3.  $(B-V)_{5kpc} \lesssim 1.4$

where  $V_{fib}$  is the V-band magnitude in an aperture matching that of the spectroscopic fiber,  $V_{tot}$  is the total V magnitude and  $(B-V)_{5kpc}$  is the colour computed from a 5 kpc aperture.

The exact cut in the colour–magnitude diagram varied slightly from cluster to cluster due to the small differences in cluster redshift and to minimize the level of contamination from the background. In a few cases, the cut has purposely included a secondary red sequence, such as for Abell 151, to be able to study also background clusters. In order to optimize the observational setup, in a few cases galaxies at fainter magnitudes or larger colours have been observed. These loose selection limits were applied so as to avoid any bias in the observed galaxy type, as is the case of a selection based on the colour–magnitude relation only (which selects only red, early type galaxies).

We computed magnitude and geometrical completeness from which we define a specific weight for each galaxy in the catalog defined as:

$$W(m, r)_i = \frac{1}{C(m)_i \cdot C(r)_i} \quad (\text{B.1})$$

Table A.1. Example of the catalog as it is made publicly available.

| WINGS ID                 | [OII]  | H $\theta$ | H $\eta$ | H $\zeta$ | CaK   | CaH   | H $\delta$ | COG   | H $\gamma$ | H $\beta$ | [OIII] | Mg    | NaD   | H $\alpha$ +N[II] |
|--------------------------|--------|------------|----------|-----------|-------|-------|------------|-------|------------|-----------|--------|-------|-------|-------------------|
| WINGSJ103833.76-085623.3 | -16.10 | 99.00      | 2.80     | 6.92      | 99.00 | -0.43 | 2.48       | 3.11  | 3.96       | -8.43     | -9.72  | 99.00 | 99.00 | -22.79            |
| WINGSJ103834.09-085719.2 | -2.40  | 99.00      | 99.00    | 99.00     | 9.06  | 99.00 | 3.61       | 99.00 | -4.87      | -1.81     | -44.32 | 2.22  | 2.72  | -37.51            |
| WINGSJ103835.89-085031.5 | -8.21  | 4.63       | 4.87     | 9.18      | 9.57  | 7.19  | 2.10       | 99.00 | -0.66      | 5.54      | 99.00  | 1.13  | 3.94  | 99.00             |
| WINGSJ103843.03-085602.8 | -17.94 | 3.55       | 3.52     | 5.08      | 4.19  | 3.72  | 99.00      | 2.38  | -1.89      | -6.38     | -3.78  | 99.00 | 1.81  | -61.90            |
| WINGSJ103848.30-084259.9 | -3.20  | -1.10      | 4.47     | 5.67      | 4.14  | 4.34  | 1.50       | 99.00 | 0.55       | 0.67      | 0.00   | 3.94  | 2.34  | -18.95            |
| WINGSJ103851.34-083738.8 | -45.25 | 99.00      | 99.00    | 2.34      | 8.18  | 2.55  | 99.00      | 99.00 | 99.00      | -1.26     | -27.04 | 3.79  | 3.07  | -43.93            |
| WINGSJ103857.45-085004.6 | -15.91 | 8.12       | 5.31     | 4.13      | 0.74  | 9.80  | 0.93       | 99.00 | 99.00      | -3.08     | -7.00  | 4.17  | 99.00 | -47.08            |
| WINGSJ103901.91-084229.6 | 99.00  | 2.44       | 99.00    | 99.00     | 4.36  | 5.49  | 2.36       | 4.76  | 99.00      | 2.97      | 99.00  | 4.06  | 2.36  | 2.60              |
| WINGSJ103905.66-085608.3 | 99.00  | 99.00      | 0.98     | 99.00     | 12.78 | 5.29  | 99.00      | 99.00 | 2.86       | -2.98     | 0.00   | 4.32  | 3.23  | 99.00             |
| WINGSJ103915.58-083903.6 | -6.36  | 6.55       | 3.01     | 5.90      | 5.41  | 6.77  | 99.00      | 5.53  | 1.00       | 6.19      | -4.10  | 1.43  | 2.89  | 999.00            |
| WINGSJ103916.50-085447.6 | -5.28  | 99.00      | 4.10     | 7.63      | 5.08  | 6.13  | 1.90       | 3.31  | 0.76       | 0.40      | 99.00  | 3.83  | 3.19  | -1.54             |
| WINGSJ103920.18-083428.7 | 99.00  | 99.00      | 8.46     | 99.00     | 6.82  | 99.00 | 3.13       | 2.86  | 1.22       | -2.39     | 99.00  | 5.12  | 2.32  | -4.58             |
| WINGSJ103920.96-084402.3 | -10.87 | 3.36       | 0.37     | 7.00      | 3.16  | 9.40  | 3.01       | 3.73  | 0.79       | 0.33      | 0.00   | 0.35  | 1.66  | -26.99            |
| WINGSJ103921.21-082823.9 | -10.78 | 4.83       | 7.45     | -1.28     | 2.48  | 11.36 | 3.42       | 0.83  | 99.00      | 0.99      | 99.00  | 99.00 | 99.00 | -11.85            |
| WINGSJ103922.27-084945.3 | -17.67 | 3.87       | 99.00    | 5.38      | 4.23  | 4.18  | 10.84      | 99.00 | 99.00      | -3.85     | -20.88 | 4.47  | 99.00 | -40.03            |
| WINGSJ103924.32-083214.7 | -20.25 | 99.00      | 99.00    | 99.00     | 3.93  | 4.15  | 7.66       | 3.36  | -5.61      | -3.33     | 99.00  | 99.00 | 0.14  | -51.25            |
| WINGSJ103924.75-084053.8 | 99.00  | 99.00      | 99.00    | 99.00     | 11.93 | 4.07  | 99.00      | 99.00 | 0.82       | -0.04     | 99.00  | 1.34  | 6.44  | 99.00             |
| WINGSJ103924.79-083011.3 | -2.25  | 6.66       | 99.00    | 3.89      | 0.21  | 99.00 | 1.86       | 7.13  | 5.17       | 5.07      | 99.00  | 0.30  | 1.29  | 99.00             |
| WINGSJ103925.05-084201.6 | -18.84 | 99.00      | 1.90     | 1.66      | 1.18  | 9.53  | 5.13       | 99.00 | 6.43       | 2.65      | -2.54  | 2.02  | 2.34  | -41.34            |
| WINGSJ103928.74-085701.4 | 99.00  | 99.00      | 99.00    | 99.00     | 99.00 | 99.00 | 3.24       | 1.51  | 1.74       | 1.51      | -10.92 | 1.74  | 5.28  | 99.00             |

| [OII] <sub>E</sub> | H $\theta$ <sub>E</sub> | H $\eta$ <sub>E</sub> | H $\zeta$ <sub>E</sub> | CaK <sub>E</sub> | CaH <sub>E</sub> | H $\delta$ <sub>E</sub> | COG <sub>E</sub> | H $\gamma$ <sub>E</sub> | H $\beta$ <sub>E</sub> | [OIII] <sub>E</sub> | Mg <sub>E</sub> | NaD <sub>E</sub> | H $\alpha$ +N[II] <sub>E</sub> | D4000 | D <sub>n</sub> 4000 | cl | C( <i>m</i> ) | C( <i>r</i> ) |
|--------------------|-------------------------|-----------------------|------------------------|------------------|------------------|-------------------------|------------------|-------------------------|------------------------|---------------------|-----------------|------------------|--------------------------------|-------|---------------------|----|---------------|---------------|
| 3.15               | 99.00                   | 1.94                  | 1.48                   | 99.00            | 0.46             | 1.14                    | 1.41             | 1.45                    | 2.44                   | 3.25                | 99.00           | 99.00            | 4.33                           | 0.95  | 0.95                | 3  | 0.1807        | 0.3237        |
| 1.66               | 99.00                   | 99.00                 | 99.00                  | 2.13             | 99.00            | 1.07                    | 99.00            | 1.86                    | 1.54                   | 13.56               | 1.85            | 1.27             | 5.98                           | 1.15  | 1.27                | 3  | 0.1807        | 0.3237        |
| 2.75               | 2.08                    | 2.74                  | 1.87                   | 1.52             | 1.40             | 0.91                    | 99.00            | 0.53                    | 1.63                   | 99.00               | 0.61            | 1.15             | 99.00                          | 2.17  | 1.99                | 3  | 0.3636        | 0.3237        |
| 4.84               | 1.45                    | 1.15                  | 1.29                   | 1.17             | 1.08             | 99.00                   | 0.75             | 0.85                    | 1.43                   | 1.40                | 99.00           | 0.77             | 5.83                           | 1.63  | 1.44                | 3  | 0.3659        | 0.3237        |
| 1.60               | 1.24                    | 1.55                  | 1.36                   | 1.30             | 1.23             | 0.78                    | 99.00            | 0.41                    | 0.63                   | 0.00                | 1.25            | 0.88             | 3.12                           | 1.51  | 1.44                | 3  | 0.3659        | 0.3237        |
| 15.90              | 99.00                   | 99.00                 | 0.75                   | 1.49             | 0.87             | 99.00                   | 99.00            | 99.00                   | 0.89                   | 4.55                | 1.23            | 0.95             | 3.90                           | 1.84  | 1.49                | 2  | 0.3636        | 0.3237        |
| 3.26               | 2.90                    | 1.68                  | 1.01                   | 0.51             | 1.57             | 0.56                    | 99.00            | 99.00                   | 1.02                   | 2.25                | 1.80            | 99.00            | 4.15                           | 1.36  | 1.24                | 3  | 0.3636        | 0.3237        |
| 99.00              | 1.89                    | 99.00                 | 99.00                  | 1.26             | 1.40             | 0.92                    | 1.27             | 99.00                   | 1.33                   | 99.00               | 1.38            | 0.93             | 0.83                           | 1.82  | 1.57                | 4  | 0.4200        | 0.3214        |
| 99.00              | 99.00                   | 99.00                 | 99.00                  | 2.95             | 1.36             | 99.00                   | 99.00            | 1.29                    | 1.22                   | 0.00                | 1.37            | 1.05             | 99.00                          | 1.78  | 1.74                | 3  | 0.3636        | 0.3237        |
| 2.51               | 1.81                    | 1.25                  | 1.47                   | 1.30             | 1.32             | 99.00                   | 2.28             | 0.59                    | 2.99                   | 1.79                | 0.66            | 0.97             | 999.00                         | 1.68  | 1.42                | 3  | 0.1807        | 0.3947        |
| 2.72               | 99.00                   | 1.53                  | 1.72                   | 1.25             | 1.52             | 0.88                    | 1.02             | 0.49                    | 0.53                   | 99.00               | 1.18            | 1.02             | 0.72                           | 1.91  | 1.66                | 3  | 0.3636        | 0.3237        |
| 99.00              | 99.00                   | 2.52                  | 99.00                  | 1.74             | 99.00            | 1.03                    | 1.20             | 0.78                    | 1.18                   | 99.00               | 1.51            | 0.91             | 1.29                           | 1.91  | 1.43                | 3  | 0.4200        | 0.2571        |
| 3.79               | 1.33                    | 0.38                  | 1.58                   | 1.09             | 1.55             | 1.13                    | 1.46             | 0.43                    | 0.37                   | 0.00                | 0.56            | 0.72             | 2.95                           | 1.52  | 1.27                | 3  | 0.3636        | 0.3947        |
| 5.49               | 2.54                    | 2.29                  | 0.83                   | 1.19             | 1.86             | 1.30                    | 0.59             | 99.00                   | 0.65                   | 99.00               | 99.00           | 99.00            | 1.97                           | 1.39  | 1.34                | 3  | 0.3636        | 0.3237        |
| 2.68               | 1.81                    | 99.00                 | 1.23                   | 1.05             | 1.18             | 1.68                    | 99.00            | 99.00                   | 1.00                   | 4.14                | 1.67            | 99.00            | 3.99                           | 1.21  | 1.18                | 1  | 0.3636        | 0.2571        |
| 5.80               | 99.00                   | 99.00                 | 99.00                  | 1.12             | 1.23             | 1.66                    | 1.23             | 1.92                    | 1.83                   | 99.00               | 99.00           | 0.46             | 4.39                           | 1.52  | 1.33                | 1  | 0.3636        | 0.2571        |
| 99.00              | 99.00                   | 99.00                 | 99.00                  | 3.69             | 1.65             | 99.00                   | 99.00            | 0.65                    | 0.46                   | 99.00               | 0.89            | 2.08             | 99.00                          | 3.85  | 3.04                | 3  | 0.3636        | 0.3571        |
| 1.96               | 2.83                    | 99.00                 | 1.18                   | 0.34             | 99.00            | 0.92                    | 1.85             | 1.69                    | 2.19                   | 99.00               | 0.55            | 0.72             | 99.00                          | 1.16  | 1.09                | 3  | 0.1807        | 0.3237        |
| 3.76               | 99.00                   | 1.30                  | 0.81                   | 0.61             | 1.69             | 1.21                    | 99.00            | 1.66                    | 1.26                   | 0.91                | 0.94            | 0.85             | 3.56                           | 1.68  | 1.42                | 1  | 0.3636        | 0.3571        |
| 99.00              | 99.00                   | 99.00                 | 99.00                  | 99.00            | 99.00            | 1.18                    | 0.96             | 0.95                    | 1.12                   | 6.55                | 0.91            | 1.40             | 99.00                          | 0.86  | 0.96                | 3  | 0.1807        | 0.3237        |

where  $C(m)_i$  and  $C(r)_i$  are the magnitude and geometrical completeness in the opportune radial and V-band magnitude bin.

The completeness as a function of magnitude is defined as:

$$C(m) = \frac{N_z}{N_{ph}}(m) \quad (\text{B.2})$$

where  $N_z$  is the number of galaxies with measured redshifts and  $N_{ph}$  is the number of galaxies in the parent photometric catalog. Completeness is usually a decreasing function of the magnitude because in observations priority was given to brighter objects.

The success rate, that is the fraction of galaxies with redshift determination with respect to the total number of observed galaxies, is similarly defined as:

$$SR(m) = \frac{N_z}{N_{tg}}(m) \quad (\text{B.3})$$

where  $N_z$  is defined as in Eq. B.2 and  $N_{tg}$  is the number of target galaxies we actually observed. Besides that, we also computed the radial completeness for our sample. It is known, in fact, that fiber collision problems can lead to a variable density of observed sources at different radii, given the fact that it is more difficult to allocate many fibers near the crowded cluster center. On the other hand, usually central parts of the clusters are privileged due to the higher density of galaxies and observers tend to allocate as many fibers as possible there. Having several fibre configurations for a given cluster, as in our case, helps mitigating the fibre collision problem even further. The net result, in our case, is a pretty flat behavior of the radial completeness function defined, analogously to the magnitude completeness, as:

$$C(r) = \frac{N_z}{N_{ph}}(r) \quad (\text{B.4})$$

with  $N_z$  and  $N_{ph}$  defined as in Eq. B.2 but for radial bins.

## Appendix C: Rejection of spectra

Due to the absence of calibration lines in the UV, several spectra taken at WHT (the “north sample”), suffer from a wavelength calibration issue affecting the wavelength range shortwards of  $\sim 4300 \text{ \AA}$ . Hence, it is often not possible to automatically recognize and properly measure a spectral line in this wavelength range, due to a displacement which, in the case of the [OII] line (which is the bluest line that we measure), can in few extreme cases reach some tens of  $\text{\AA}$ . Since this displacement is not only wavelength dependent, but it may also vary from spectrum to spectrum, it is not possible to automatically correct for this effect in a straightforward way. The fact that it is not always possible to properly measure some of the lines that typically characterize the stellar populations, can make the automatic/blind spectral fitting, which was the main reason for having a reliable EW measure (Fritz et al., 2007, 2011), meaningless in some cases.

To recover as much information as possible, and use as many spectra as we could from the north sample, we proceeded as follows. After running our fitting procedure over the entire north sample, we measured the EW of the four most prominent UV lines, namely [OII], the two calcium

lines (H and K; 3969 and 3934  $\text{\AA}$ , respectively), and H $\delta$ . This was done manually for each of these four lines and for each spectrum displaying the calibration problem. Due to these issues, care must be taken when judging the quality of a fit by means of the  $\chi^2$  value only. We recalculate a  $\chi^2$  by only considering spectral features (i.e. lines and continuum emission) longwards of 4300  $\text{\AA}$ , and rejected all the spectra with a  $\chi^2_\nu > 3$ . On the remaining spectra, we checked that the values which we have manually measured were compatible with those of the best fit model. When this was the case the fit, together with the derived physical quantities (e.g. stellar mass, star formation rate, etc.) was considered to be acceptable, and the spectrum considered in the analysis.

Furthermore, since after the selection procedure described above, some of the clusters from the north sample were very poorly sampled only having a few galaxies that are spectroscopically confirmed members (Cava et al., 2009), we decided not to include, in all of the statistical studies that will follow in the paper, those clusters with a number of confirmed members less than 20. This leaves us with only 7 clusters of the north sample, still containing more than 50% of the usable spectra from this catalog.